TESTS OF A RADIATIVE TRANSFER MODEL FOR NUMERICAL PREDICTION OF THE ATMOSPHERIC GENERAL CIRCULATION

Robert John Plante

NAVAL POSTGRADUATE SCHOOL
Monterey, California

THESIS

TESTS OF A RADIATIVE TRANSFER MODEL
FOR NUMERICAL PREDICTION
OF THE ATMOSPHERIC GENERAL CIRCULATION

by

Robert John Plante

Thesis Advisor: F. L. Martin

March 1973

Tests of a Radiative Transfer Model for Numerical Prediction of the Atmospheric General Circulation

by

Robert John Plante
Lieutenant, United States Navy
B.S., Illinois Institute of Technology, 1966

Submitted in partial fulfillment of the
requirements for the degree of

MASTER OF SCIENCE IN METEOROLOGY

from the

NAVAL POSTGRADUATE SCHOOL
March 1973

ACKNOWLEDGEMENTS

The author wishes to express his appreciation to his advisor, Professor F. L. Martin, for his suggestions, advice, guidance and support in this research.

Appreciation is also expressed to Professor Robert L. Haney for numerous discussions on various facets of the subject matter and for his suggestions especially on the oceanic heat budget.

ABSTRACT

An evaluation is performed of a radiation model for the Naval Postgraduate School primitive-equation numerical weather prediction system. The model employs empirical expressions for atmospheric absorptivity, scattering-reflectivity, cloud-reflectivity and earth-surface reflectivity to compute solar insolation absorbed at earth and in the key atmospheric layers. The terrestrial cooling effect at earth and in these same key atmospheric layers is formulated using recent empirically-derived emissivities for the effects of both water vapor and CO_2.

Mean seasonal atmospheric soundings for the Northern Hemisphere are utilized for testing the model. In addition, application of atmospheric boundary-layer modeling permits determination of the surface-layer turbulent transports (in the vertical) of sensible and latent heat at the earth's surface. To evaluate the validity of the radiation model, heat budgets are compiled for the earth-atmosphere system, the atmospheric column and the earth's surface.

TABLE OF CONTENTS

LIST OF TABLES

LIST OF FIGURES

I. INTRODUCTION

The present study was to evaluate a radiation package for the Naval Postgraduate School primitive equation prediction model. The radiation package is primarily an outgrowth of the model used in the UCLA general circulation model (Gates et al. 1971) with modifications suggested from the NCAR model (Oliger et al. 1970) and from the Geophysical Fluid Dynamical Laboratory (Manabe and Strickler, 1964).

The model consists of five σ-levels ($\sigma = P/\pi$ where π is the surface pressure) for the purposes of data input as shown in Figure 1. Cloud cover was treated by the use of a single cloud layer extending from $\sigma = 0.8$ to 0.4. In the computations for both pressure-scaled water-vapor and CO_2 absorber masses, a more realistic method was introduced to extrapolate accurate water-vapor values above levels normally available from radiosonde data ($P \approx 300$ mb). A system for the integrations of net terrestrial flux was introduced by using empirically derived absorptivities (Sasamori, 1968) based on the radiation chart of Yamamoto (1952), for water-vapor and CO_2. Evaporation and sensible heat fluxes were derived from a formulation for surface layer heat transfer by Langlois and Kwok (1969).

Northern hemisphere climatological atmospheric data from London (1957) were utilized to evaluate the model.

Pressure, temperature, and relative humidity data were divided into the four seasons and available over ten degree latitude bands from the equator poleward.

The development of the terrestrial fluxes is given in Section III and the solar radiation model is given in Section IV. The results of the computed long and short wave fluxes were then compared to those of Budyko (1955), London (1957) and Katayama (1967).

Finally, to evaluate the adaptability of the radiative package to a general circulation model, three heat budgets were attempted. The budgets were for the earth-atmosphere system, the atmospheric column and the surface. Since heat transfer calculations due to evaporation and sensible heat are more easily made over ocean surfaces, London's atmospheric data was fitted to climatological ocean surface temperature and wind data from the United States Weather Bureau's Atlas of Climatic Charts of the Oceans (1938). Surface layer evaporation and sensible heat flux computations were not conducted poleward of 60N because of the possibility of ice cover. Rather, combined evaporation and sensible heat rates were taken from Vowinckel and Taylor (1964).

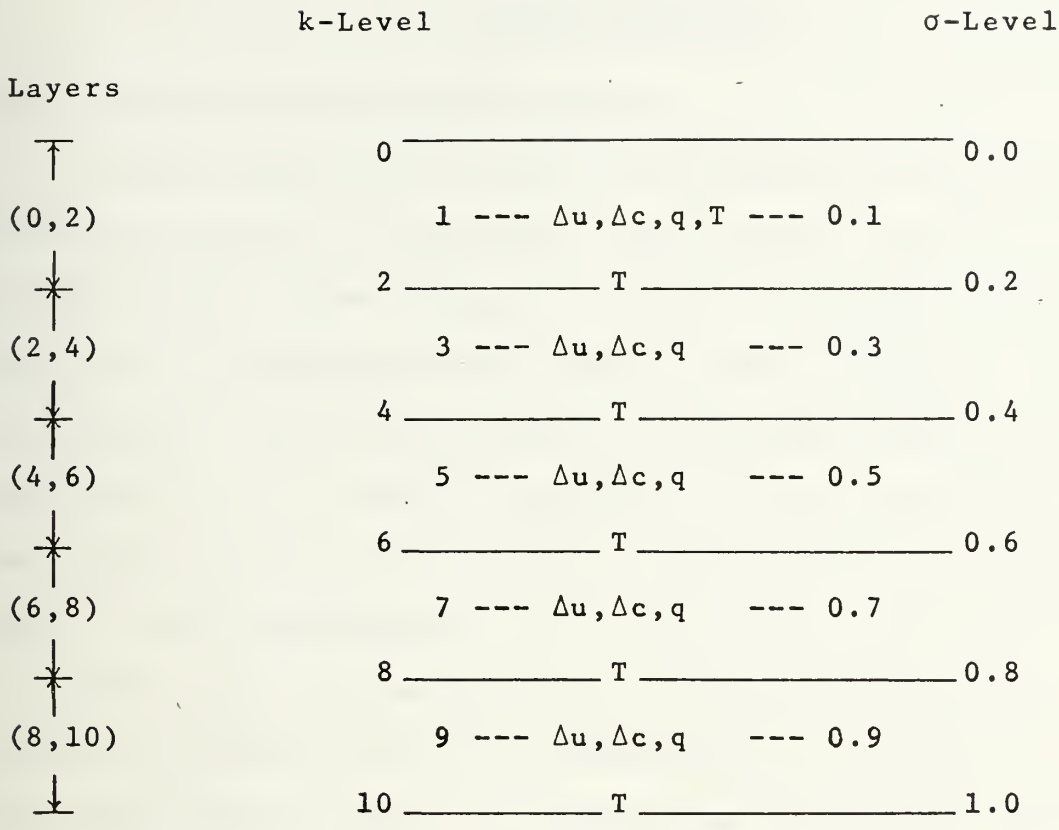

Figure 1. Representation of the five-layer sounding model used for radiative transfer calculations. Temperature, mixing ratio, pressure-scaled water-vapor (Δu) and CO_2 (Δc) absorber mass increments are shown at the appropriate σ-levels and k-levels ($k = 10\sigma$).

II. DATA PREPARATION

A. TEMPERATURE AND MOISTURE TERMS

Northern hemisphere vertical and latitudinal distributions of pressure, temperature, and relative humidity were taken from the climatological soundings of London (1957). The data was compiled in four mean seasonal tables. The latitudinal variation consisted of 10 degree latitude bands measured from the equator northward. In the vertical, data was distributed at 1 km intervals from the surface to the base of the stratosphere.

With actual radiosonde data, continuous information would be available above the tropopause to at least the 0.1 sigma level. The $\sigma = 0.1$ level was the highest level at which the water-vapor mixing ratio was considered to be recoverable from the fields of q. London's radiosonde data was continuous only to the tropopause. Since the tropopause varies in height latitudinally as well as seasonally, adjustment of the vertical distribution of T and q had to be made to insure that the data would be available to $\sigma = 0.1$ level. The simplest solution for the stratosphere was to assume isothermal conditions with constant relative humidity to the $\sigma = 0.1$ level for any vertical sounding that ended below $\sigma = 0.1$.

It was necessary to interpolate from the distribution at successive km levels in the vertical (as listed in

London, 1957) to the specific sigma levels of Figure 1. Temperatures were carried at the 1.0, 0.8, 0.6, 0.4, 0.2 and 0.1 σ-levels. Since surface data was available in London's soundings, T_{10} was set equal to the listed surface temperature rather than requiring an extrapolation of the type

$$T_{10} = 0.5\ (3T_9 - T_7) \qquad (1)$$

Temperatures at other sigma surfaces, say at level k, were interpolated using a three-point Lagrangian formula of the form

$$\begin{aligned} T(k) = {} & (T_2)(P_k-P_1)(P_k-P_0)/(P_2-P_1)(P_2-P_0) \\ & + (T_1)(P_k-P_2)(P_k-P_0)/(P_1-P_2)(P_1-P_0) \\ & + (T_0)(P_k-P_1)(P_k-P_2)/(P_0-P_2)(P_0-P_1) \end{aligned} \qquad (2)$$

where it is assumed that the data level (P_0,T_0) lies above the σ-level in question and (P_2,T_2) lies below that level.

Mixing ratio values were calculated with London's data using

$$q = RH\ (0.622e_s)/P \qquad (3)$$

The q-values were then interpolated to σ_k-levels using the Lagrangian formulation of (2) applied to q's at known levels. The q_k-values were centered at the odd σ-levels of 0.9, 0.7, 0.5 and 0.3. These values are then considered to be the layer means between the even σ-levels.

Accurate humidity information is in general not available above σ = 0.3, especially in the stratosphere. To find a mean q-value representative of the layer (0,2) a different formulation was used.

Smith (1966) has shown a strong correlation between $q(P)$ and the surface value q_{10} through the extrapolative formula

$$\frac{q(P)}{q_{10}} = \left(\frac{P}{P_{10}}\right)^{\lambda} \qquad (4)$$

London's soundings were tested to obtain a best-fit between ln q and ln P of the form

$$\frac{q(P)}{q_3} = \left(\frac{P}{P_3}\right)^{\lambda} \qquad (5)$$

which is similar in form to that suggested by Smith. The values of $q(P)$ resulting from (5) for $\sigma = 0.9$, 0.7, 0.5 and 0.3 were used to solve for the profile parameter λ. This parameter varied with latitude and season as shown in Table I. The relationship (5), with appropriate λ-values, was then used to extrapolate q at $\sigma = 0.1$. The resulting q_1-values were then considered the mean q-values for each layer (0,2).

The procedure just described to derive q_1 was regarded as justifiable in view of the following reasons:

(i) The residuals $[q(\text{est}) - q(\text{obs})]_k$ were small for all $k \geq 3$, and

(ii) The extrapolated q_1 corresponds to the proper order of magnitude as listed in model atmospheres (Valley, 1965) at pressures $P \approx 100$ mb.

TABLE I. Seasonal and latitudinal values of the profile parameter λ of Equation (5).

Latitude	Winter	Spring	Summer	Fall
0-10	3.1438	3.0178	3.2885	3.0202
10-20	3.1182	3.3024	3.4381	3.2555
20-30	3.1205	3.3978	3.4272	3.2374
30-40	2.6437	3.3838	3.3563	3.0873
40-50	3.0002	3.5178	3.2480	3.1259
50-60	2.7210	3.2382	3.2031	3.1846
60-70	2.3267	2.7478	3.0684	2.8925
70-80	1.9671	2.1953	2.7886	2.4617
80-90	1.1743	1.7831	2.8434	2.1262

B. CLOUD MODELING

In both the solar and terrestrial radiative transfer processes, it is essential to know the fractional cloud cover (CL) at each grid point. Clouds act as almost perfect blackbody radiators for infrared radiation, and as efficent reflectors for solar radiation.

There is a difficulty in parameterizing different cloud types and heights. In this model, as in the UCLA general circulation model, only a single cloud layer was parameterized for the purposes of inclusion in the vertical radiative transfer model at gridpoints. As is done in most other numerical prediction schemes involving cloud amount, CL, use is made of Smagorinsky's (1960) algorithm (applicable at approximately 700 mb)

$$CL = 2.0\ (e/e_g) - 0.7 \qquad (6)$$

where $0 \leq CL \leq 1.0$. When a cloud amount $CL > 0$ existed, it was assumed to extend between $\sigma = 0.8$ to $\sigma = 0.4$.

Comparison of the calculated values of CL computed from (6) and those tabulated from seasonal climatological estimates by Telegadas and London (1954) and Seinde (1954) showed a marked difference in the mid-latitudes as seen by comparison of Tables II and III. Since other climatological estimates of cloud cover, namely Sellers (1965), compared best with the data tabulated in Table II, climatology was used in this model rather than the results of Table III.

TABLE II. The seasonal distribution of total cloudiness (percent cloud cover) tabulated by London (1957).

Lat N.	Winter	Spring	Summer	Fall
0-10	47	51	54	53
10-20	36	42	49	48
20-30	38	42	42	41
30-40	50	52	41	46
40-50	59	59	55	56
50-60	63	62	63	66
60-70	58	60	66	70
70-80	47	59	69	70
80-90	40	55	64	60

TABLE III.The seasonal distribution of total cloudiness (percent of sky cover) calculated by the Smagorinsky algorithm.

Lat N	Winter	Spring	Summer	Fall
0-10	30	40	56	46
10-20	12	20	48	36
20-30	10	10	30	20
30-40	18	14	22	16
40-50	34	26	30	26
50-60	42	34	42	42
60-70	46	40	50	46
70-80	46	38	50	48
80-90	34	28	50	40

Even though London's cloud-cover climatology was accepted as valid here, it should be realized that London's results included overlapping clouds at multiple levels, which was impossible with the parameterization using (6). An improved cloud model permitting cloud existence at two or more levels in the vertical should be attempted in future radiative heating systems. At the present time, the added complexity of the radiative physics is considered too costly in computer time for inclusion in the present model. However, it should be noted that Arakawa et al. (1972) have already developed the concept of a three-layer radiative cloud model for a 1972 version of the UCLA general circulation model.

Another reason for the choice of the climatological CL must be considered. With the use of climatology, transient synoptic scale perturbations and disturbances in the soundings are smoothed or eliminated. Therefore, the day-to-day variations of relative humidity tend to be smoothed out during the season. The resulting smoothed relative humidity distributions thus tended to be less than their normal peak-values and give too small a magnitude of CL when employing the Smagorinsky algorithm.

C. ABSORBER-MASS DEFINITIONS: PRESSURE SCALED

Since mixing ratio values have now been computed at the five odd σ-levels (Figure 1), it is possible to determine the pressure-scaled water-vapor absorber masses,

Δu_k, associated with the five corresponding layers. This is done in the model in such a way that the additive scheme

$$u(6,10) = u(8,10) + u(8,6) \qquad (7)$$

holds. The layer water vapor absorber mass, u(2k, 2k-2), has been centered at odd levels (2k-1). The scaled absorber mass is calculated using

$$\Delta u_{2k-1} = \frac{q_{2k-1}\,\Delta P}{g}\left(\frac{P_{2k-1}}{P_0}\right)^{0.72} \qquad (8)$$

which, as has been noted, is the absorber mass in the layer (2k, 2k-2). ΔP is a constant in the analysis scheme equal to 0.2π. The mixing ratio value, q_{2k-1}, is the mean centered value in the layer (2k, 2k-2). The pressure ratio factor $(P_{2k-1}/P_0)^{0.72}$ is the scaling factor for collisonal line-broadening after Möller and Raschke (1964). This latter formulation disposes of the necessity of temperature scaling in the usual Lorentz line-broadening formula (c.f., Danard, 1969), where the pressure-ratio scaling is linear and a temperature-ratio scaling factor is indicated by $(T/T_0)^{-0.5}$ times the N.T.P. mass within a layer. The subscript "0" denotes an N.T.P. condition where P_0 = 1013.25 mb, T_0 = 273.16°K, and ρ_0 is the N.T.P. value of density.

If (8) is integrated from $P_{2k} = (0.2k)\,P_0$ to $P = \pi$, the result is

$$u_{2k} = (\pi/P_0)^{1.72}\left(\frac{P_0}{1.72g}\right)\sum_{n=5}^{n=k\geq 1}\bar{q}_{2n-1}\left[\sigma_{2n}^{1.72} - \sigma_{2n-2}^{1.72}\right] \qquad (9)$$

where by definition

$$\sigma_k \equiv P_{2k}/\pi \equiv \frac{P_{2k}}{P_0}\frac{P_0}{\pi} \qquad (10)$$

For CO_2, Möller and Raschke (1964) proposed pressure-scaling similar to that of water-vapor but with a pressure-ratio exponent of 0.65. For simplicity, a single pressure-scaling exponent of 0.72 was utilized for both cases. The form of the layer-reduced absorber mass of CO_2 in N.T.P. cm/cm^2 in the layer (2k, 2k-2) is

$$\Delta c_{2k-1} = 3.14 \times 10^{-4} \left(\Delta P/g\rho_0\right)\left(\frac{P_{2k-1}}{P_0}\right)^{0.72} \qquad (11)$$

The process of integration from P_{2k} to P_0 yields the formulation

$$c_{2k} = \frac{3.14 \times 10^{-4}}{1.72} H\left[1 - \frac{P_{2k}}{P_0}^{1.72}\right] \qquad (12)$$

where $H = 7.995 \times 10^5$ cm is the height of the homogeneous atmosphere in N.T.P. cms. Adjusting (12) to a σ-coordinate system with $P = \pi$ at the surface yields

$$c_{2k} = \frac{3.14 \times 10^{-4}}{1.72} H\left(\frac{\pi}{P_0}\right)^{1.72}\left[1 - \sigma_{2k}^{1.72}\right] \qquad (13)$$

Table IV shows the seasonal distribution of the total pressure-scaled water-vapor absorber masses, u(0,10). As expected, the summer season contains the largest absorber mass with the least in winter. Spring and fall values are intermediate between the maximum and minimum values. Computations for the CO_2 absorber-masses are dependent upon

TABLE IV. Seasonal distributions of total pressure-scaled water-vapor masses, u(0,10), in gm cm^{-2}.

Latitude	Spring	Summer	Fall	Winter
0-10	3.878	4.287	4.023	3.624
10-20	3.271	4.316	3.826	2.749
20-30	2.417	3.601	3.055	1.993
30-40	1.607	2.897	2.133	1.279
40-50	1.099	2.292	1.426	0.747
50-60	0.703	1.793	0.932	0.449
60-70	0.437	1.428	0.598	0.256
70-80	0.289	1.045	0.471	0.163
80-90	0.192	0.901	0.319	0.105

the total mass of air in a unit column, and hence on the surface pressure. Since the variation in surface pressure averaged across all latitude bands was less than 10 mb, the CO_2 absorber-masses were nearly constant [$c(0,10) \doteq 125$ cm/cm^2].

III. TERRESTRIAL RADIATIVE TRANSFER

A. THEORETICAL AND EMPIRICAL BACKGROUND

Virtually all of the radiation packages in present use with large scale circulation models in the United States [cf., Manabe and Strickler (1964), Oliger et al. (1970), Arakawa et al. (1969)] make use of Yamamoto's (1952) water-vapor flux emissivities as a basis for their long-wave radiative flux calculations. The water-vapor flux emissivity is normally thought of as a function of both water-vapor scaled mass and temperature. Yet, in the normal range of temperatures ($T \geq 220K$), the emissivity is virtually independent of temperature. At temperatures $T < 220K$, the wave-averaged flux emissivity is defined after Yamamoto (1952) by

$$\varepsilon(u,T) = \frac{\int_o^\infty [1-\tau_{F\nu}(1_{\nu o}u)] \frac{dB_\nu}{dT}(T=220K)\, d\nu}{\int_o^\infty \frac{dB_\nu}{dT}(\nu,T)\, d\nu} \qquad (14)$$

Here the numerator has its temperature dependent terms fixed at 220K, while the denominator equals $4St(T^3)$ even when $T<220K$. The temperature affects the population of different rotational energy levels within the so-called "rotational" band. At low temperatures, Planck's function shifts maximal radiant energy to the longer wavelengths in the rotational band, according to Wien's displacement

law of

$$\lambda_{max} = 2897/T \qquad (15)$$

where λ_{max} is in microns. Thus with T < 220K, the highly absorbed rotational lines are the only contributors to water-vapor absorptivity. This leads to an increase of absorption near the center of the rotational band and thus to an increase in mean absorptivity with decreasing temperature. This phenomenon is depicted graphically in Figure 2 after Sasamori (1968).

Yamamoto's radiation chart has been the basis of most recent radiation calculations. Sasamori (1968, 1970) used Yamamoto's radiation theory to write empirical formulas for all of the emissivities needed for long-wave radiative flux calculations. These empirical formulas have been shown by Sasamori to yield adequate accuracy and were adapted for this numerical study. The temperature independent emissivity for water-vapor, from Sasamori, is given by

$$\varepsilon(u) = 0.24 \log_{10}(u + 0.010) + 0.622 \qquad (16)$$

This formulation was used for T $\geq$ 220K. For T < 220K, Sasamori gives the temperature-dependent part of the emissivity function by water vapor as

$$\varepsilon(u,T)=(8.34T^{0.353\log_{10}u-0.44})u^{-0.3455\log_{10}u-.705} \qquad (17)$$

When absorption by CO_2 and water-vapor are considered jointly, the product law of transmissivities must be employed. In doing this, the transmissivity of the two

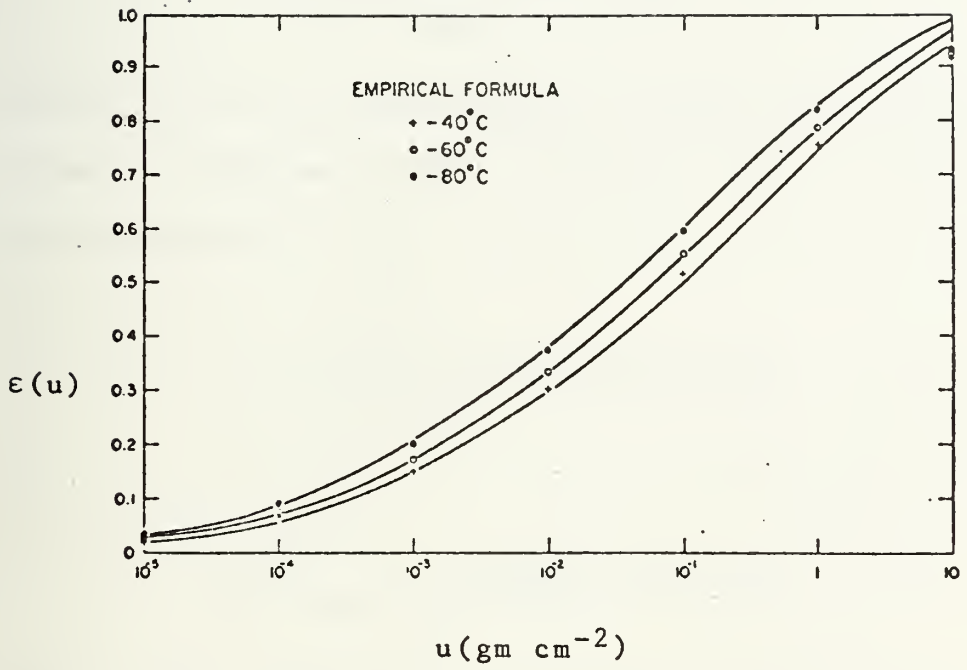

Figure 2. Temperature dependent part of the emissivity with varied amounts of scaled water-vapor.

absorbers acting jointly may be expressed as

$$\tau_F(u,c) = \tau_F(u)\tau_F(c) \tag{18}$$

The flux integral as formulated by Yamamoto is

$$F = \int_{u=0,T_{Ref}}^{u(T)} \varepsilon(u,T)\, dB \tag{19}$$

where u(T) is the water-vapor sounding mass measured away from the reference level. Equation (19) then becomes with the inclusion of CO_2

$$F = \int_{u=0,c=0}^{u,c(T)} [1-\tau_F(u)\tau_F(c)]dB \tag{20}$$

or

$$F = \int_{u=0,c=0}^{u,c} [\varepsilon(u,T) + \Delta\varepsilon]\, dB \tag{21}$$

The $\Delta\varepsilon$ term represents the effective emission due to CO_2 not already counted in the water-vapor flux calculations. The added emission is expressed on the Yamamoto chart by an increase of emissivity at all points of the radiative sounding (except at the reference level points). The $\Delta\varepsilon$ term includes only the 15μm band emitted flux of CO_2 which has not already been counted in emission by overlap with the rotational band of water vapor. Sasamori considered this CO_2 band emissivity to be temperature independent in developing the empirical formulation

$$\Delta\varepsilon = 0.07262[1-0.62556(u+0.286)^{0.26}][\log c+1.064] \tag{22}$$

In the following flux computations, the emissivity, ε, will include both the effects of CO_2 given by (22) and that of water vapor given in (16) and (17).

B. TECHNIQUES OF NET FLUX COMPUTATIONS

Schematic representations of the Yamamoto radiation chart were utilized for considering the integration of the net long wave flux calculations. In Figure 3, the hatched area is a representation of downward flux at the surface. The area may be computed using the trapezoidal summation rule as follows:

$$F\downarrow(10) = 0.5\{[\varepsilon(8\text{-}10)(B_{10}-B_8)]+[\varepsilon(8\text{-}10)+\varepsilon(6\text{-}10)](B_8-B_6)+[\varepsilon(6\text{-}10)+\varepsilon(4\text{-}10)](B_6-B_4)+[\varepsilon(4\text{-}10)+\varepsilon(2\text{-}10)](B_4-B_2)+[\varepsilon(1\text{-}10)+\varepsilon(2\text{-}10)](B_2-B_1)+2\int_{B=0}^{B(T_1)}\bar{\varepsilon}[(0\text{-}10),T]db\} \quad (23)$$

Here $B = St * T^4$ is the Stefan-Boltzmann blackbody flux and $\varepsilon(8\text{-}10)$, for example, represents the emissivity computed from Sasamori's empirical equations using the water vapor and CO_2 present in the layer (8-10). The term $\bar{\varepsilon} = \varepsilon(u,T) + \Delta\varepsilon$ is solved by $\varepsilon(u,T)$ given by (17) and $\Delta\varepsilon$ by (22). The subscripts on the Stefan-Boltzmann fluxes (i.e., $B_{10} - B_8$) are identifers for the layer contribution from which the flux-emission takes place.

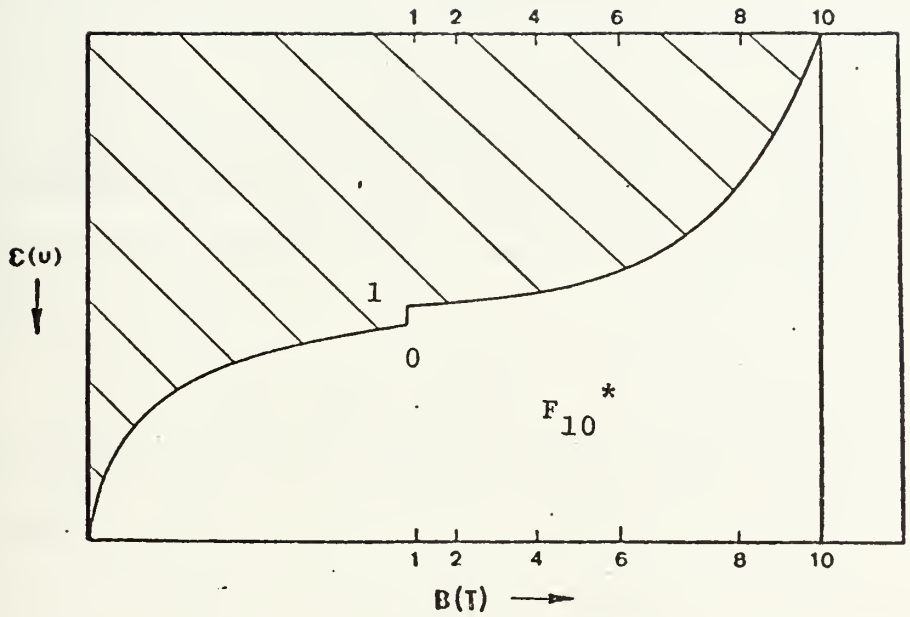

Figure 3. Schematic area-depiction of net flux at level 10.

The final integral of (23), $\int_{B=0}^{B(T_1)} \bar{\varepsilon}\, dB$,

may be evaluated by the integrated result

$$St * T_1^4 \{\bar{\varepsilon}(u_o,T_1)\left(\frac{8.0}{0.353 \log_{10} u_o + 3.56}\right) + 0.07262[1-0.62556(u_o + 0.286)^{0.26}][\log_{10} c_o + 1.064]\} \quad (24)$$

In (24), it is understood that the integration spans the temperature range $(0,T_1)$ along the final isopleths u_o and c_o (e.g., Figure 3). The net flux at level 10 is given by

$$F_{10}^{*} = B_{10} - F\downarrow(10) \quad (25)$$

where the asterisk superscript denotes F(up) - F(down) at the level.

The net flux at level 6 is represented schematically by B_{10} minus the hatched area in Figure 4. The numerical modeling follows (23) where

$$F_6^{*} = B_{10} - 0.5 \{\varepsilon(6\text{-}8)(B_8 - B_6) + [\varepsilon(6\text{-}8) + \varepsilon(6\text{-}10)](B_{10} - B_8) + \varepsilon(4\text{-}6)(B_6 - B_4) + [\varepsilon(4\text{-}6) + \varepsilon(2\text{-}6)](B_4 - B_2) + [\varepsilon(2\text{-}6) + \varepsilon(1\text{-}6)](B_2 - B_1) + 2 \int_{B=0}^{B(T_o)} \bar{\varepsilon}[(0\text{-}6), T]\, dB\} \quad (26)$$

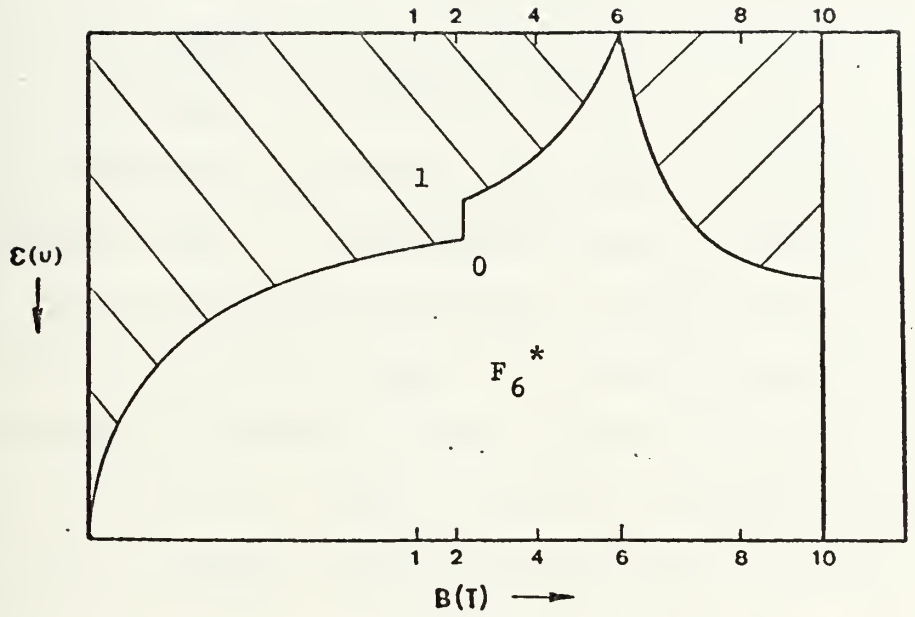

Figure 4. Schematic area-depiction of net flux at level 6.

Figure 5 is the schematic for net flux at level 2. Following the previous computations

$$F_2^* = B_{10} - 0.5\{\varepsilon(2\text{-}4)(B_4-B_2)+[\varepsilon(2\text{-}4)+\varepsilon(2\text{-}6)](B_6-B_4)+[\varepsilon(2\text{-}6)+\varepsilon(2\text{-}8)](B_8-B_6)+[\varepsilon(2\text{-}8)+\varepsilon(2\text{-}10)](B_{10}-B_8)+\varepsilon(1\text{-}2)(B_2-B_1)+2\int_{B=0}^{B(T_1)}\bar{\varepsilon}\,[(0\text{-}2),T]\,dB\} \quad (27)$$

The foregoing net fluxes F_{10}^*, F_6^*, F_2^* are clear sky calculations only. A modification due to cloudy skies is made. The cloud-covered fraction is given by CL and the clear sky fraction is (1-CL). The cloud-covered fraction is considered an overcast which extends vertically from level 8 to level 4. Figure 6 shows a schematic flux diagram, after Yamamoto (1952), of net fluxes at levels 10 and 2, when only the overcast sky fraction is considered. The horizontally hatched area is now the net flux at level 10. The net flux at level 6 is zero since a layer of approximately 50 meters in depth with average cloud droplet content may be regarded as a blackbody (Brunt, 1939) at the mean temperature of the cloud layer. The net flux at level 2 is the slant hatched area in the diagram.

The net flux at level 10, with overcast skies is given by

$$F_{10}^* = (B_{10} - B_8)(1 - 0.5\varepsilon(8\text{-}10)) \quad (28)$$

Normally (28) represents a cooling effect at the earth's surface. At the same time, the net flux at level 8, or the

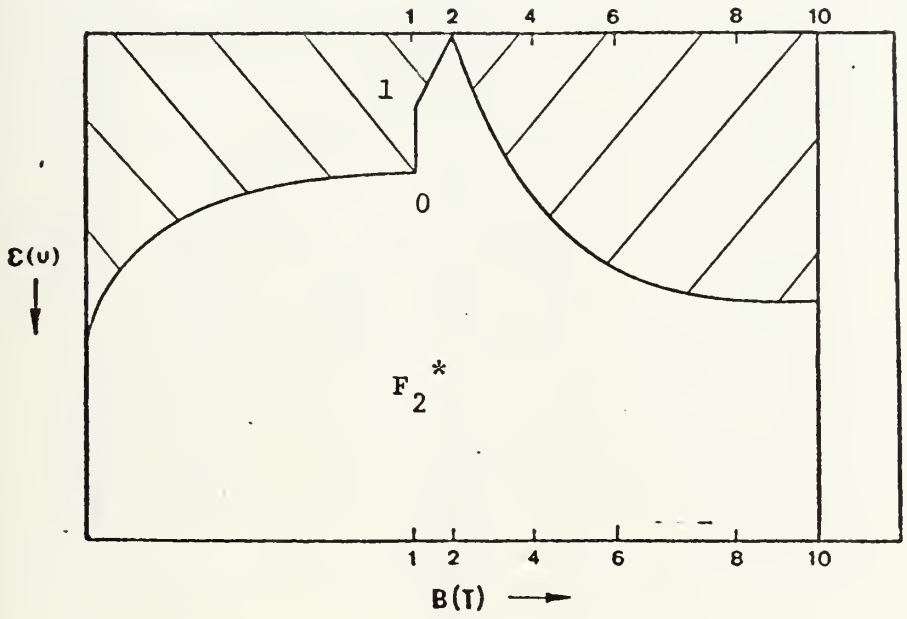

Figure 5. Schematic area-depiction of net flux at level 2.

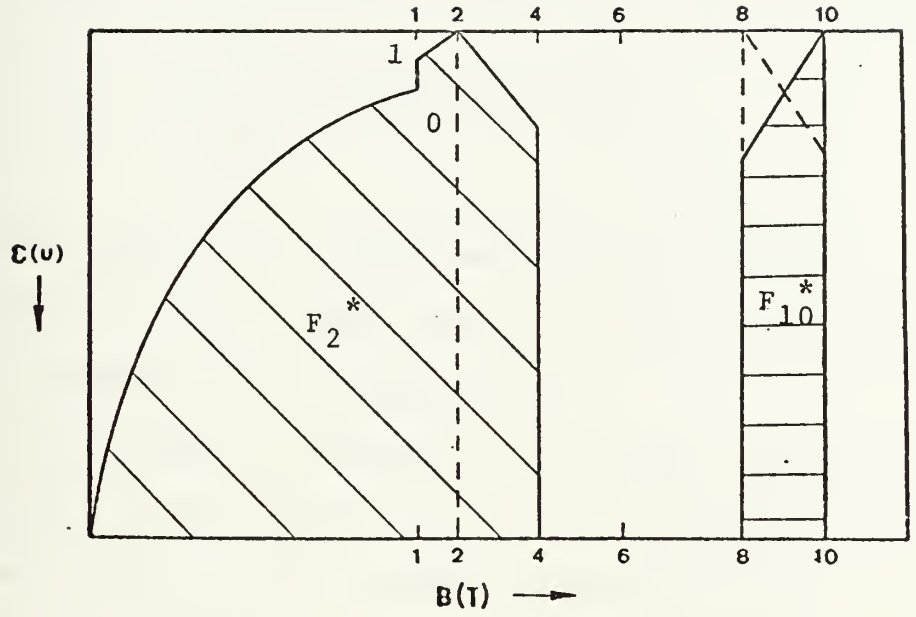

Figure 6. Schematic area-depiction of net flux at reference levels 10 and 2 when an overcast cloud extends between levels 8 and 4.

cloud base, is an equal magnitude (Fig. 6) so that the layer (8-10) has zero flux divergence. However, the cloud base receives a net flux warming equal in magnitude to F_{10}^*

The net flux at level 2 for the overcast case is given by

$$F_2^* = B_4 - 0.5\{\varepsilon(2\text{-}4)(B_4 - B_2) + \varepsilon(1\text{-}2)(B_2 - B_1) + 2 \int_{B=0}^{B(T_1)} \bar{\varepsilon}[(0\text{-}2), T]\, dB\} \quad (29)$$

This net flux, F_2^*, is much smaller than that for clear skies because of the lead term B_4 on the right side of (29) as contrasted with B_{10} in (27).

The net fluxes, computed at the three reference levels, must now be cloud-weighted to yield final results for net long-wave flux transfer across the interface by

$$F_{10}^* = [F_{10}^*(28)]\ CL + [F_{10}^*(25)](1\text{-}CL) \quad (30)$$

$$F_6^* = [F_6^*(26)]\ (1 - CL) \quad (31)$$

$$F_2^* = [F_2^*(29)]\ CL + [F_2^*(27)](1\text{-}CL) \quad (32)$$

The temperature-dependent flux integral denoted by $\int \bar{\varepsilon}\,(u_o, T_1)\, dB$ was evaluated for an entire range of final T_1 and u_o values which could occur in the atmosphere. These results are listed in Appendix Table A-1.

C. DIVERGENCE OF NET FLUX AND RESULTANT COOLING RATES

The resultant, cloud weighted, seasonal distributions of net flux at the three reference levels of σ = 0.2, 0.6,

and 1.0 are listed in Tables V(a-d). The 24-hour temperature changes between the reference levels due to terrestrial radiation alone are also listed. The mean radiative temperature change centered at the midpoint of the column was computed by the first law of thermodynamics so that the cooling rate for the layer (6,10) is

$$-\frac{\partial T}{\partial t} = (F_6^* - F_{10}^*)/0.4\pi \frac{1000}{g} c_p \qquad (33)$$

and for the layer (2,6) is

$$-\frac{\partial T}{\partial t} = (F_2^* - F_6^*)/0.4\pi \frac{1000}{g} c_p , \qquad (34)$$

where π is surface pressure in mb.

To compare the accuracy of the long-wave calculations, the meridionally averaged mean values for the fluxes at the levels $\sigma = 0.2$ and 1.0 were computed. The result was represented by the percentage of the meridionally averaged insolation at the top of the troposphere. Katayama's 63 percent (1967), and London's 62 percent (1957) for net flux at 200mb are in good agreement with the 64 percent from this study. The net flux at the surface was 18 percent for all three studies. Converting these spatially averaged results to annual means (ly day^{-1}), we get a net outgoing radiation at $P \approx 200$ mb of 430 from the Katayama-London means compared to our 450. At the surface, the net outgoing long-wave radiation is 120 (ly day^{-1}) compared to our 131.

In the net flux calculations, a comparison was made between three different atmospheric situations in order to evaluate the contribution of cloudiness to the total outgoing flux from the earth-atmosphere system. One test considered

TABLE V(a). Net long wave flux (ly day^{-1}) distributions with latitude at reference levels σ = 0.2, 0.6 and 1.0 with the radiative temperature cooling (°C day^{-1}) between reference levels with average total cloud cover. (Spring)

Latitude	0-10	10-20	20-30	30-40	40-50	50-60	60-70	70-80	80-90
F_2^*	488	510	499	449	410	378	344	313	304
ΔT °C/24 Hr Layer (2,6)	2.89	2.57	2.47	2.52	2.53	2.42	2.14	1.95	1.83
F_6^*	203	255	253	198	158	137	132	118	120
ΔT °C/24 Hr Layer (6,10)	0.62	0.95	0.97	0.66	0.43	0.31	0.39	0.48	0.46
F_{10}^*	142	161	157	133	116	106	93	70	75

TABLE V(b). Net long wave flux (ly day^{-1}) distributions with latitude at reference levels σ = 0.2, 0.6 and 1.0 with radiative temperature cooling (°C day^{-1}) between reference levels, with average total cloud cover. (Summer)

Latitude	0-10	10-20	20-30	30-40	40-50	50-60	60-70	70-80	80-90
F_2^*	491	506	511	499	461	420	395	370	366
ΔT °C day^{-1} Layer (2,6)	3.07	2.95	2.65	2.47	2.80	2.82	2.72	2.64	2.43
F_6^*	187	215	249	249	183	141	126	108	127
ΔT °C day^{-1} Layer (6,10)	0.43	0.69	0.93	1.04	0.66	0.39	0.27	0.25	0.43
F_{10}^*	145	146	157	145	118	103	100	83	82

TABLE V(c). Net long wave flux (ly day^{-1}) distributions with latitude at reference levels σ = 0.2, 0.6 and 1.0 with radiative temperature cooling (°C day^{-1}) between reference levels, with average total cloud cover. (Fall)

Latitude	0-10	10-20	20-30	30-40	40-50	50-60	60-70	70-80	80-90
F_2^*	478	501	504	478	422	379	343	319	308
ΔT °C day^{-1} Layer (2,6)	2.88	2.81	2.49	2.55	2.55	2.59	2.47	2.22	1.90
F_6^*	193	223	256	224	168	123	99	98	119
ΔT °C day^{-1} Layer (6,10)	0.57	0.71	0.97	0.78	0.57	0.26	0.21	0.23	0.48
F_{10}^*	136	152	159	146	111	97	78	76	72

TABLE V(d). Net long wave flux (ly day^{-1}) distributions with latitude at reference levels σ = 0.2, 0.6 and 1.0 with radiative temperature cooling (°C day^{-1}) between reference levels, with average total cloud cover. (Winter)

Latitude	0-10	10-20	20-30	30-40	40-50	50-60	60-70	70-80	80-90
F_2^*	516	525	490	408	374	338	308	294	265
ΔT °C day^{-1} Layer (2,6)	2.96	2.48	2.24	2.12	2.30	2.20	1.90	1.56	1.21
F_6^*	223	279	267	196	145	119	119	139	145
ΔT °C day^{-1} Layer (6,10)	0.63	1.00	1.01	0.70	0.45	0.37	0.52	0.58	0.55
F_{10}^*	161	180	166	126	101	83	68	81	90

only clear skies, another had average cloudiness and the third tested totally the overcast model. Results were compiled in mean annual latitudinal distributions of long-wave net flux in Tables VI(a-c).

Since temperatures normally decrease with height in the atmosphere, a positive net flux occurred at all levels. Strong surface temperature inversions can lead to negative F_{10}^{*}, but these conditions were not present in this study. Also, in an atmosphere where the effective optical depth decreased sharply with height, the net radiative flux increases sharply with height at the levels of the decreased water-vapor mass. This happens primarily because most of the emitted flux from the lower layer passes upwards unattenuated by the dry upper layers.

The net flux through the tropopause is larger at all latitudes for clear skies than for conditions of average or overcast cloudiness. This occurs because the net outgoing radiation comes from a lower, and therefore warmer layer in the case of clear skies. In the case of overcast skies, the radiating layer is the cloud top at $\sigma = 0.4$ Rather than $\sigma = 1.0$ for clear skies. The tropopause net flux with average cloudiness is a weighted average between the overcast and clear-sky cases of Table VI.

The largest variability of net flux magnitudes with cloud cover occurred at the $\sigma = 0.6$ level. The minimum value of zero is observed during total cloudiness since this level lies within the cloud layer which was treated as a blackbody. Maximum values occurred of course in conditions of clear skies.

TABLE VI(a). Mean annual radiative long-wave flux (ly day^{-1}) normal cloud cover.

Latitude	0-10	10-20	20-30	30-40	40-50	50-60	60-70	70-80	80-90
F_2^*	493	511	501	457	427	379	348	324	311
F_6^*	201	241	256	192	164	130	119	116	152
F_{10}^*	146	160	160	138	112	97	85	78	80

TABLE VI(b). Mean annual radiative long-wave flux (ly day^{-1}) clear sky.

Latitude	0-10	10-20	20-30	30-40	40-50	50-60	60-70	70-80	80-90
F_2^*	577	586	571	533	505	469	424	387	362
F_6^*	413	431	432	411	382	357	329	307	288
F_{10}^*	222	226	223	210	197	191	179	169	163

TABLE VI(c). Mean annual radiative long-wave flux (ly day^{-1} overcast cloud cover.

Latitude	0-10	10-20	20-30	30-40	40-50	50-60	60-70	70-80	80-90
F_2^*	413	413	399	374	351	327	305	288	272
F_6^*	0	0	0	0	0	0	0	0	0
F_{10}^*	74	75	68	56	48	44	30	19	10

IV. SOLAR RADIATION TREATMENT

A. EFFECTIVE SOLAR INSOLATION

The solar radiation treatment is not as straightforward. Following Joseph (1966), a solar constant of 2.00 ly min^{-1} was assumed. A 4% attenuation by oxygen and ozone above the tropopause was assumed which gave an effective solar constant of 1.92 ly min^{-1}. The effective tropopause height was assumed to be at $\sigma = 0.2$.

The effective insolation at the tropopause was computed from

$$F = S(r/r_m)^{-2} \quad D \overline{\cos \theta} \qquad (35)$$

where

S = effective solar constant

r/r_m = radius vector of earth relative to the sun

θ = zenith angle of sun relative to observing point

$\overline{\cos \theta}$ = daily average of cos θ

D = fractional length of daytime

The (r/r_m) is listed as a function of the Julian date in the Smithsonian Meteorological Tables (List, 1958). The following table, after Manabe and Möller (1961) was employed to derive the daily mean cos θ and duration of insolation as a function of latitude and time of the year. Computations of F were based upon mean mid-seasonal values of

Spring - April 15th

Summer - July 15th

TABLE VII. The seasonal and latitudinal distributions of duration of insolation and daily mean values of cos θ.

Lat.	Fractional Length of Daytime				Weighted Mean cos θ			
	Apr	Jul	Oct	Jan	Apr	Jul	Oct	Jan
5	.508	.517	.500	.496	.625	.587	.614	.591
15	.521	.537	.492	.471	.618	.601	.579	.549
25	.533	.562	.483	.450	.599	.593	.524	.474
35	.546	.596	.471	.421	.558	.567	.458	.393
45	.562	.637	.454	.362	.501	.521	.379	.317
55	.596	.708	.437	.321	.423	.453	.282	.203
65	.629	.837	.404	.208	.345	.369	.176	.106
75	.750	1.000	.329	-	.241	.311	.071	-
85	1.000	1.000	-	-	.168	.318	-	-

TABLE VIII. Incoming solar radiation on a horizontal surface at the top of the tropopause (ly day^{-1}).

Latitude	Spring	Summer	Fall	Winter
0-10	884	867	844	784
10-20	896	922	783	692
20-30	889	952	696	571
30-40	848	965	593	443
40-50	784	948	473	306
50-60	702	916	339	174
60-70	604	882	195	59
70-80	503	888	64	0
80-90	468	908	0	0

Fall - October 15th

Winter - January 15th

Joseph's method (1966) was followed in partitioning the effective solar insolation into a part subject to water-vapor absorption but not to Rayleigh scattering, and the remainder subject to only Rayleigh scattering. The presence of clouds introduced cloud reflectivities in both portions. Thus, the solar insolation subject to tropospheric absorption comprises wavelengths $\geq$ 0.9 μm and was obtained from

$$F_A = 0.349F \tag{36}$$

In the wavelengths $\leq$ 0.9 μm, water vapor absorption is negligible and the solar insolation subject to Rayleigh scattering was obtained from

$$F_S = 0.651F \tag{37}$$

B. DISPOSITION OF FLUX SUBJECT TO SCATTERING

In treating the fraction of the solar insolation subject to scattering, Joseph (1966), found that the Rayleigh scattering values at sea level in clear skies (after Coulson, 1959) could be fitted by least squares to the form

$$\alpha_S = 0.085 + 0.25074 \log \left(\frac{\pi}{p_o} \sec \theta\right) \tag{38}$$

where π is the observed surface pressure. For a full-day the value of sec θ in (38) was treated as $\overline{\sec \theta}$, the time-mean sec θ, which was taken as the inverse of the mean $\overline{\cos \theta}$ values from Table VII.

Another reflective parameter is the surface albedo, α_g. After numerical experimentation designed to test for a global radiative heat balance, a constant average surface albedo of $\alpha_g = 0.14$ was deduced. It should be noted that this value of α_g turned out to be equal to that deduced by Budyko (1955). A discussion of the validity of a constant surface albedo will be reserved for the surface balance section.

Considering the possibility of multiple reflections between earth and atmosphere, each of which diverts downward the fraction α_s of the earth surface reflectance α_g, the clear sky insolation at earth after scattering is given by

$$I_{SO} = F_S(1-\alpha_S)[1+\alpha_S\alpha_g+---(\alpha_S\alpha_g)^n+ ---](1-\alpha_g) \qquad (39)$$

or

$$I_{SO} = F_S(1-\alpha_S)(1-\alpha_g)/(1-\alpha_S\alpha_g) \qquad (40)$$

For the existence of a cloud cover, the Rayleigh reflection coefficient of (38) was applied at the cloud top $\sigma = 0.4$, rather than $\sigma = 1$. At the cloud top, a unique cloud reflectivity fraction R_c of 0.5 was chosen everywhere. This reflection is basically a Mie-type, diffuse backscattering caused by water droplets in the clouds.

Thus, at the cloud top, the entering solar-beam insolation is given by

$$F_{SC4} = \frac{F_S[1-\alpha_S(\frac{0.4\pi}{P_o} \sec\theta)](1-R_c)}{1-\alpha_S R_c} \qquad (41)$$

This downward scattered beam is forced into a diffuse angular array by the Mie scattering process. In order to

account for further attenuation by Rayleigh scattering when the ray paths are diffuse, a mean slant path angle θ_D such that sec θ_D = 5/3 was judged more appropriate than the actual sec θ (Katayama, 1966).

The Rayleigh scattering coefficient beneath the cloud top (i.e. in layer (4,10)) was found to be

$$\alpha_{SD} = \alpha_{SD_{10}} - \alpha_{SD_4} = 0.25074 \log 2.5 \qquad (42)$$

Thus, α_{SD} below the cloud top has a constant value of 0.0998. In this connection, it may be noted that Manabe and Strickler (1964) employed a constant value of $\alpha_S = 0.07\ S\ \overline{\cos\ \theta}$ loss to space by Rayleigh scattering regardless of the presence of clouds.

Multiple reflections take place below the cloud top. Martin (1972) has shown that upon simplification, the insolation at earth after cloudy-sky scattering is

$$I_{SC} = F_{SC4}(1-\alpha_{SD})(1-\alpha_g) + \frac{F_{SC4}[\alpha_{SD}+\alpha_g(1-\alpha_{SD})](1-\alpha_{SD})(1-\alpha_g)R_c}{[1-R_c(1-\alpha_{SD})^2\ \alpha_g]} \qquad (43)$$

In the above accounting, certain small atmospheric reflection terms occurring in the direction cloud to earth (or reverse) have been ignored as small compared to the air transmission factor $(1 - \alpha_{SD})$.

Finally, the weighted mean earth-surface absorption of the scattered solar beam becomes

$$I_S(10) = (1-CL)I_{SO} + I_{SC}(CL) \qquad (44)$$

where I_{SO} is given in (40) and I_{SC} in (43).

C. TROPOSPHERIC ABSORPTION OF SOLAR RADIATION

In considering the absorption of the F_A component of solar insolation, the Manabe-Möller solar-absorptivity function

$$a = 0.0946\ (u_{2,2K}\ \sec\theta)^{0.303} \qquad (45)$$

was used. The form of Equation 45 indicates that the absorption function a is applied over the pressure-scaled water vapor mass in the layer (2,2K) along the zenith path of slant angle θ. Restricting absorption to the ratio 0.349F requires that the multiplicative constant 0.0946 of (45) be adjusted to (0.0946/0.349) = 0.271.

The absorbed insolation in the layer (2,6) is then

$$A(2,6) = 0.271[u(2,6)\sec\theta]^{0.303}\ F_A \qquad (46)$$

Similarly, the absorbed insolation in the layer (2,10) is

$$A(2,10) = 0.271[u(2,10)\sec\theta]^{0.303} F_A \qquad (47)$$

Therefore, the absorbed insolation in the layer (6,10) is given by

$$A(6,10) = A(2,10) - A(2,6) \qquad (48)$$

Since the amount of solar beam absorbed in the layer (2,10) is available by (47), the solar insolation in the F_A-partition received at earth is given by $F_A - A(2,10)$. This portion is reduced by ground albedo α_g so that the earth-absorbed insolation resulting from F_A is

$$I_{AO}(10) = F_A\{1-0.271[u(2,10)\sec\theta]^{0.303}\}(1-\alpha_g) \qquad (49)$$

A modification is made for cloudy skies. The absorption in the layer (2,4) was computed according to the Manabe-Möller absorptivity function [Equation (46)]. The solar beam at level 0.4 is given by

$$F_A(4) = F_A - A(2,4) \tag{50}$$

Of the F_A-energy available at level $\sigma = 0.4$, the fraction $(1-R_c)$ is transmitted through the cloud top. Thus

$$F_A(4) = [F_A - A(2,4)](1-R_c) \tag{51}$$

Within the cloud layer, the water vapor path below $\sigma = 0.4$ is subject to the mean diffuse-path augmentation factor 5/3 (after Katayama, 1966).

Inside the cloud layer, another variable has been introduced. The value is u_c or equivalent water vapor mass for droplet absorption in clouds. The values of the absorption coefficient a_{CLD} due solely to cloud particles have been taken after theoretical computations of Korb, Michalowski and Möller (1956). These values are listed after Manabe and Strickler (1964, p. 367) in Table IX, below.

TABLE IX. Absorptivities (a_{CLD}) of cloud droplets.

Latitude Band	a_{CLD}
0-39N, low-to-middle clouds	0.035
40-64N, low-to-middle clouds	0.020
65-90N, ice-crystal clouds	0.005

Since only a single cloud layer was used in the radiative model, the larger absorptivities associated with the larger water content was identified with the 0-39N latitude

band of Table IX. The values of a_{CLD} are due solely to absorption by either liquid water or the solid ice content of clouds. The values of a_{CLD} are considered mean values for the latitude bands shown in Table IX. Moreover, the a_{CLD} values of Table IX are averaged for the entire solar beam, and not merely for the F_A portion of the insolation. Hence, the value of a_{CLD} has been multiplied by (1.0/0.349) for application to the F_A-partition. In this spectral region, the effective cloud-water absorptivities become

$$a^* = 2.8653\ a_{CLD} \tag{52}$$

or

$$a^* = \{\tfrac{5}{3}(u(4,8)+u_c)]^{0.303} - [\tfrac{5}{3}u(4,8)]^{0.303}\}0.271 \tag{53}$$

Equation (53) may be solved for u_c as a function of a^* and $u(4,8)$

$$\frac{u_c}{u(4,8)} = \{[1+ \frac{a^*}{0.271}(\frac{0.6}{u(4,8)})^{0.303}]\ ^{3.003} - 1.0\} \tag{54}$$

Values of u_c were computed as a function of u(4,8) for the latitudes of Table IX and are shown in Appendix Table B.

With u_c known, the following calculations are made

$$A(4,6) = F_A(4)\{0.271[\tfrac{5}{3}\,u(4,6) + \frac{u_c}{2}]^{0.303}\} \tag{55}$$

$$A(6,10) = F_A(4)\{0.271[\tfrac{5}{3}(u(4,10)+u_c)]^{0.303}\} - A(4,6) \tag{56}$$

where $F_A(4)$ is evaluated upon entering the cloud top. Finally, the insolation reaching earth after absorption in cloudy skies is

$$I'_{AC}(10) = F_A(4) - A(4,6) - A(6,10) \tag{57}$$

With the surface albedo effect $(1-\alpha_g)$ included, the earth-absorbed part of $I'_{AC}(10)$ becomes

$$I_{AC}(10) = I'_{AC}(10)\ [(1-\alpha_g)/(1-\alpha_g R_c)] \qquad (58)$$

D. NET INSOLATION ABSORBED AT EARTH

The weighted sum for the insolation at earth after absorption is given by

$$I_{AC}(10) = CL[I_{AC} \text{ of } (58)] + (1-CL)[I_{AO} \text{ of } (49)] \qquad (59)$$

Thus the total insolation absorbed at earth is given by

$$Q_{10} = I_A(10) + I_S(10) \qquad (60)$$

The resulting values of Q_{10} are listed in Table X.

E. COMPARISON OF MERIDIONALLY AVERAGED RADIATION QUANTITIES

In order to compare the various annual outputs of this radiation model with the results of other researchers, the radiational quantities derived by the NPS model were time-averaged and space-averaged over the Northern Hemisphere. The resulting global mean annual quantities are compared with the results by Katayama (1967), Budyko (1956) and London (1957). The mean values are presented as a percentage of the solar radiation at the top of the troposphere.

Meridionally-averaged values were generated using the formulation

$$\bar{R} = \frac{2\pi \int_{\phi_1}^{\phi_2} a^2 R \cos\phi \, d\phi}{2\pi \int_{\phi_1}^{\phi_2} a^2 \cos\phi \, d\phi} \qquad (61)$$

TABLE X. Seasonal distribution of insolation absorbed at earth (Q_{10}) in ly day^{-1}.

Latitude	Spring	Summer	Fall	Winter
0-10	451	430	424	409
10-20	484	471	404	385
20-30	487	510	374	316
30-40	450	525	315	234
40-50	405	484	241	157
50-60	361	451	166	88
60-70	317	430	95	30
70-80	264	430	31	0
80-90	248	454	0	0

where

R = annual mean radiative quantity at latitude ϕ

a = radius of earth

ϕ = center of the latitude band under consideration

$d\phi$ = latitude increment in degrees between successive bands. This increment is a constant of 10° for this study.

The formulation in Equation (61) may be reduced to a series summation using cosine weighting factors as indicated in

$$\bar{R} = \frac{\sum_{n=1}^{9} R \cos \phi_n}{\sum_{n=1}^{9} \cos \phi_n} \qquad (62)$$

where $\phi_1 = 5°$, $\phi_2 = 15°$, etc.

When the results of this study are compared with those of Katayama, Budyko, and London in Table XI, it is found that they are in rather good agreement as a whole. However, there are some minor differences. First, the older model estimates of solar radiation absorbed in the atmosphere are generally 3 to 5 units higher than determined by this study. Also, while the average global albedo, $A_p(\phi)$, determined in this study is typical of usual values quoted, namely 34%, the meridional distribution of $A_p(\phi)$ was more nearly uniform with respect to ϕ than would have resulted if the means had been based upon hourly computations for the months involved. This result leads to a lower than normal value of solar radiation absorbed at the surface in low latitudes and a

TABLE XI. Comparison of meridionally averaged values of radiation quantities. The values are presented as percentages of the global mean insolation at the top of the troposphere.

	Katayama	Budyko	London	Plante
Solar radiation at top of troposphere	100	100	100	100
Solar radiation absorbed in atmosphere	18	16	14	13
Global albedo	37	40	35	34
Solar radiation absorbed at surface	45	44	47	52
Outgoing long-wave radiation at 200 mb	63	60	62	64
Outgoing long-wave radiation at surface	18	17	18	18
Sensible and latent heat flux (see Section IX)	29	27	29	31

larger than typical value at the surface in high latitudes. The reason for this is basically threefold: First, atmospheric absorption by dust was not considered in the NPS model, since it is essentially a predictive model. However, London (1957) applied the results of Houghton (1954) who used atmospheric transmissivity due to dust as given by

$$\tau_D \approx (0.95)^m \tag{63}$$

where $m = \sec \theta$, represents the air mass traversed by the solar beam. London's depletion by atmospheric dust would then be given by

$$D = (1 - \tau_D) \tag{64}$$

of which 25% is considered subject to absorption. Even so, the contribution of dust absorption is small and can generally be considered of the order of 1%, which is approximately the difference between the NPS absorption figure and that of London's.

Another contribution to absorption not previously considered here is secondary absorption of the reflected portion of the solar beam. Since the reflected portion of the solar beam above clouds is subject to the same percentage absorption as the incoming beam, the error in absorption may be as high as 1% of the incoming solar radiation. Neither London's study nor this study considered secondary absorption of the reflected beam and consequently the resulting atmospheric absorptions are closely comparable. Katayama considered secondary absorption following a first reflection

of the solar beam by a cloud or by ground or both. As a result Katayama's solar absorption in air was the largest of the four cases considered.

The third consideration is Katayama's cloud cover. In the Katayama radiative study, a larger climatological cloud cover was considered than in the present study, or that of London or Budyko. The cloud amounts were generally characteristic of coverages over the oceans (after McDonald, 1938) rather than a combined ocean-continent regime.

It is not exactly clear how Katayama allowed McDonald's overlapping cloud-layers to be combined, although he constrained the total cloud-coverage to agree with that of Sir Napier Shaw's (1936). The significant feature of the greater cloud coverages is that they afford not only greater solar absorptivity but also a greater global albedo as postulated by Katayama's empirical formulas

$$A_c = A_\infty \, [1-\exp(-b_1 \, h)] \tag{65}$$

$$R_c = R_\infty \, [1-\exp(-b_2 \, h)] \tag{66}$$

where h is the cloud thickness and b_1, b_2, A_∞, R_∞ are characteristic values for a given cloud type. Thus Katayama finds a greater cloud absorptivity than was found by London or Plante (Table XI) as well as a larger global albedo because of the larger cloud coverages.

F. GLOBAL ALBEDO CONSIDERATIONS

In the process of deriving the transmission of the two solar components F_A and F_S, the following dispositional terms were discussed:

(i) the combined insolation rate at the tropopause denoted by F of Equation (35).

(ii) the absorption rate of insolation in the atmosphere

(iii) the absorption rate of insolation, Q_{10}, at earth

With these terms, the reflected insolational rate from planet earth, as a function of latitude and season may be computed. This rate may be denoted by A_pF, where A_p is the global albedo. The term A_pF must be identified as the difference of

$$F - A(2,10) - Q_{10} = A_pF \qquad (67)$$

It should be noted that three significant reflective parameters have affected the value of the left side of (67) namely the sky albedo, the cloud albedo ($R_c = 0.5$), and the earth-surface albedo, α_g. For simplicity, the latter two were held constant at reasonably well accepted figures independent of latitude. While direct computations of the right side of (67) were made at each step of computing (ii) and (iii), the resulting global albedo values must also be consistent with the values inferred from the left side of (67).

A note of caution in regard to comparing global albedo as shown in Table XI. A correct mean global albedo may distort the atmospheric heat balance if not distributed correctly with respect to latitude. For example, if a meridional bias exists in the computed global albedo, A_p,

with too large a value at low latitudes and too small a value at high latitudes, the result will influence the poleward heat transport required for balance, after independent computation of latent and sensible heat transfers across the earth-air interface (see Section IX). This type of bias in global albedo appears to have developed in this study presumably by oversimplifying the ray-paths in clouds. Choosing a single mean path through clouds for a given representative day, and time of year seems to have overestimated the global albedo in this study in lower latitudes while underestimating it at high latitudes.

V. RADIATIVE TEMPERATURE CHANGES

Long-wave radiation, with a normal temperature lapse, will lead to a cooling of the atmosphere as seen as seasonal distributions in Tables V(a-d). In certain locations and seasons, some of the atmospheric layers considered were subject to temperature inversions which led to local heating rather than the usual cooling. Another heating situation examined was at an overcast cloud base. The terminology, 'cloud base warming' or 'green house effect' may be used to describe this phenomenon. Since the net flux within a cloud layer is zero, a negative net flux increment existed in the cloud to sub-cloud layer (8,10). With the sign convention adopted here, this represents a base-warming effect. In the cloud top region, there is a substantial net flux increment $F_2^* - F_6^*$ which leads to considerable cloud-top cooling. Thus, in infrared radiative temperature changes the role of clouds is clearly to increase the cooling rate at the cloud tops and to decrease the cooling rate at the cloud bases. This process can be considered as a decrease of the atmospheric stability within the cloud layer.

The mean annual infrared temperature changes in the troposphere are plotted in Figure 7 as a function of latitude. The dependency of these cooling rates upon the climatological cloud cover at these same latitudes is evident by

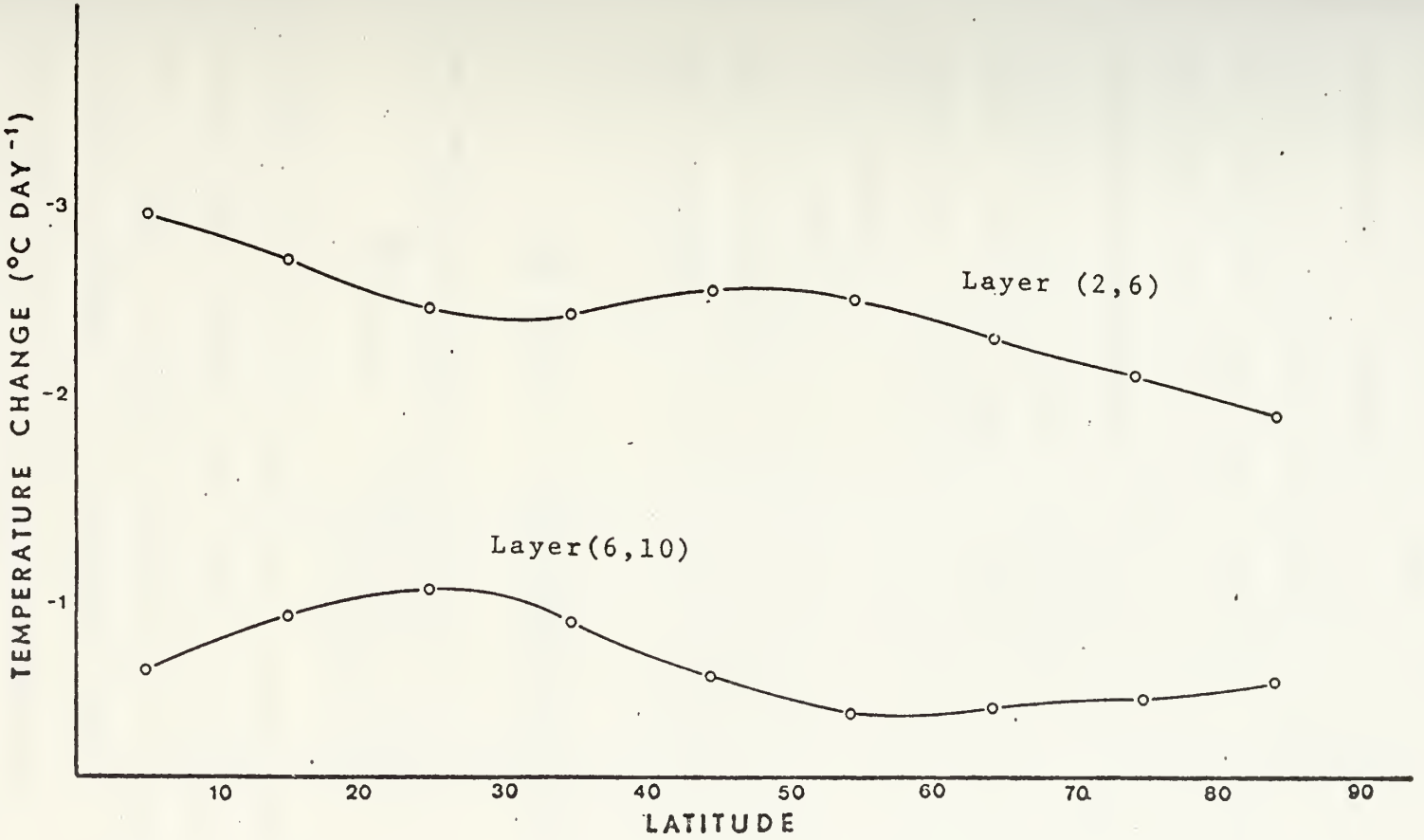

Figure 7. Mean annual infrared cooling rate in layers (6,10) and (2,6) with average cloud cover.

inspecting Figure 8. A linear regression was performed relating the mean long-wave temperature changes of each troposphere layer against the total cloud cover used in the computation at latitude ϕ. Each latitude band for each season was considered separately, giving a total of 36 cases. For the layer (6,10) the correlation coefficient was -0.95 while for the layer (2,6) the correlation was +0.99. Graphs showing the comparison of temperature changes found with clear and with average cloudy skies for the layer (2,6) and layer (6,10) are shown in Figures 9 and 10, and clearly demonstrate the phenomena of cloud-top cooling and cloud-base warming.

In conditions of normal cloudiness, the infrared heat losses are partially offset by atmospheric absorption of solar radiation. The resultant temperature change in the layer (6,10) is

$$\frac{\partial T}{\partial t}(6,10) = \frac{-(F_6^* - F_{10}^*) + A(6,10)}{0.4\pi(1000/g)\, c_p} \qquad (68)$$

The temperature change in the layer (2,6) is given by

$$\frac{\partial T}{\partial t}(6,10) = \frac{-(F_2^* - F_6^*) + A(2,6)}{0.4\pi(1000/g)\, c_p} \qquad (69)$$

In most cases, this absorption of solar insolation is smaller than the cooling that results from long wave radiation and acts only to modify the pattern of radiative heat loss, as shown in Figure 11. The dashed curves represent the annual mean rate of temperature change due to long wave radiative cooling for the layers (6,10) and (2,6). The

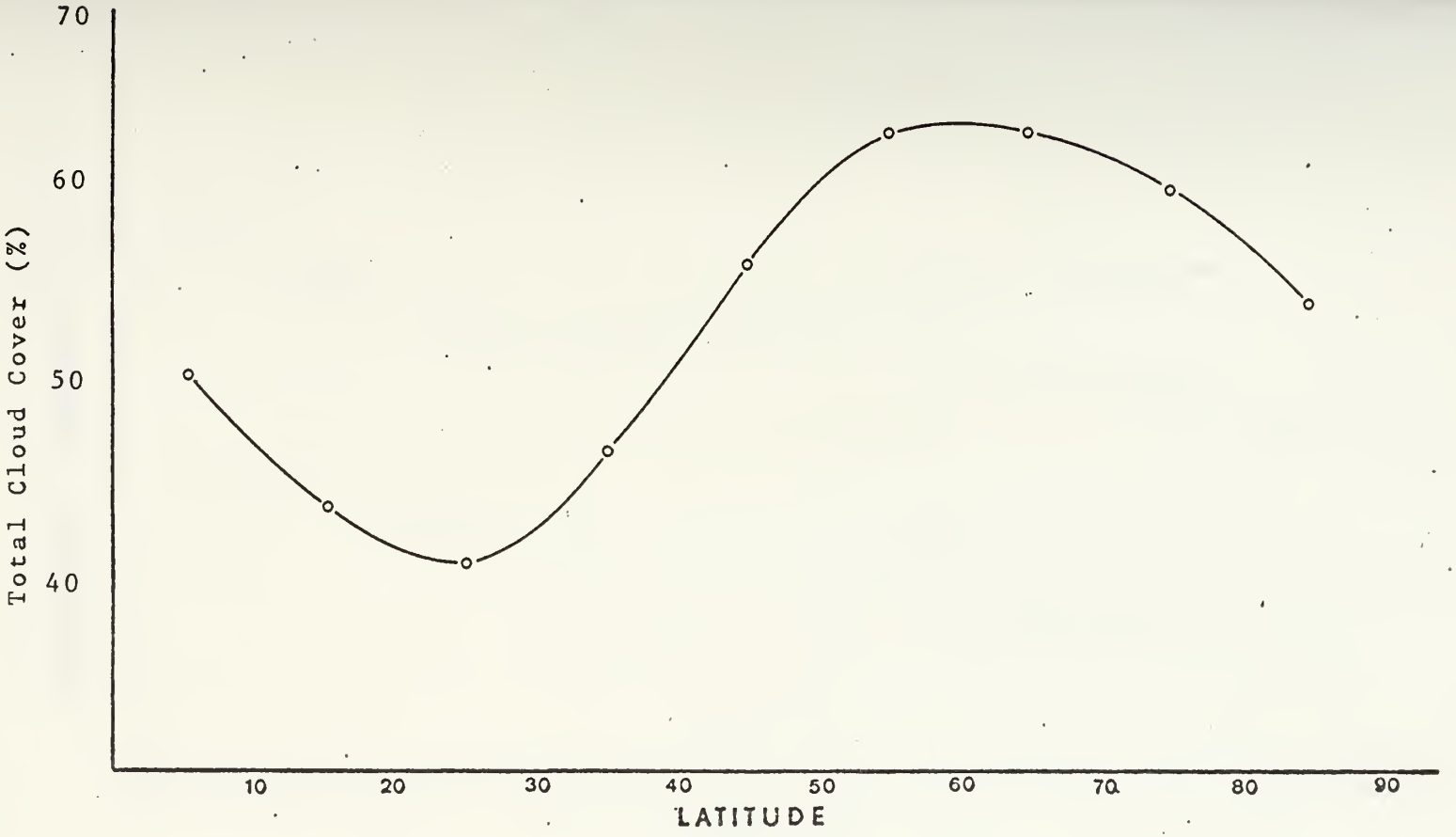

Figure 8. Mean annual cloud cover distribution with latitude.

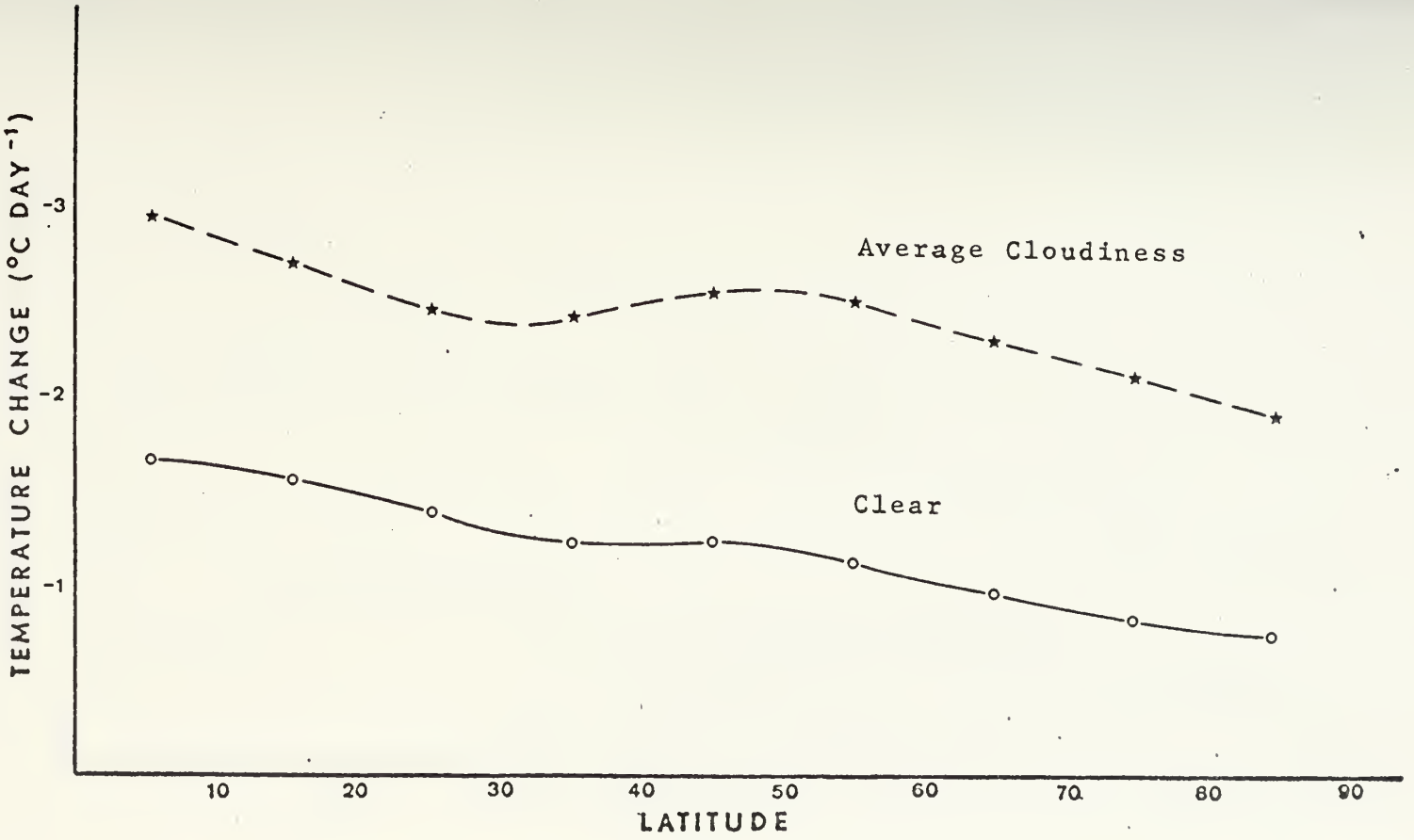

Figure 9. Mean annual infrared cooling rate in layer (2,6) with clear and average cloudy skies.

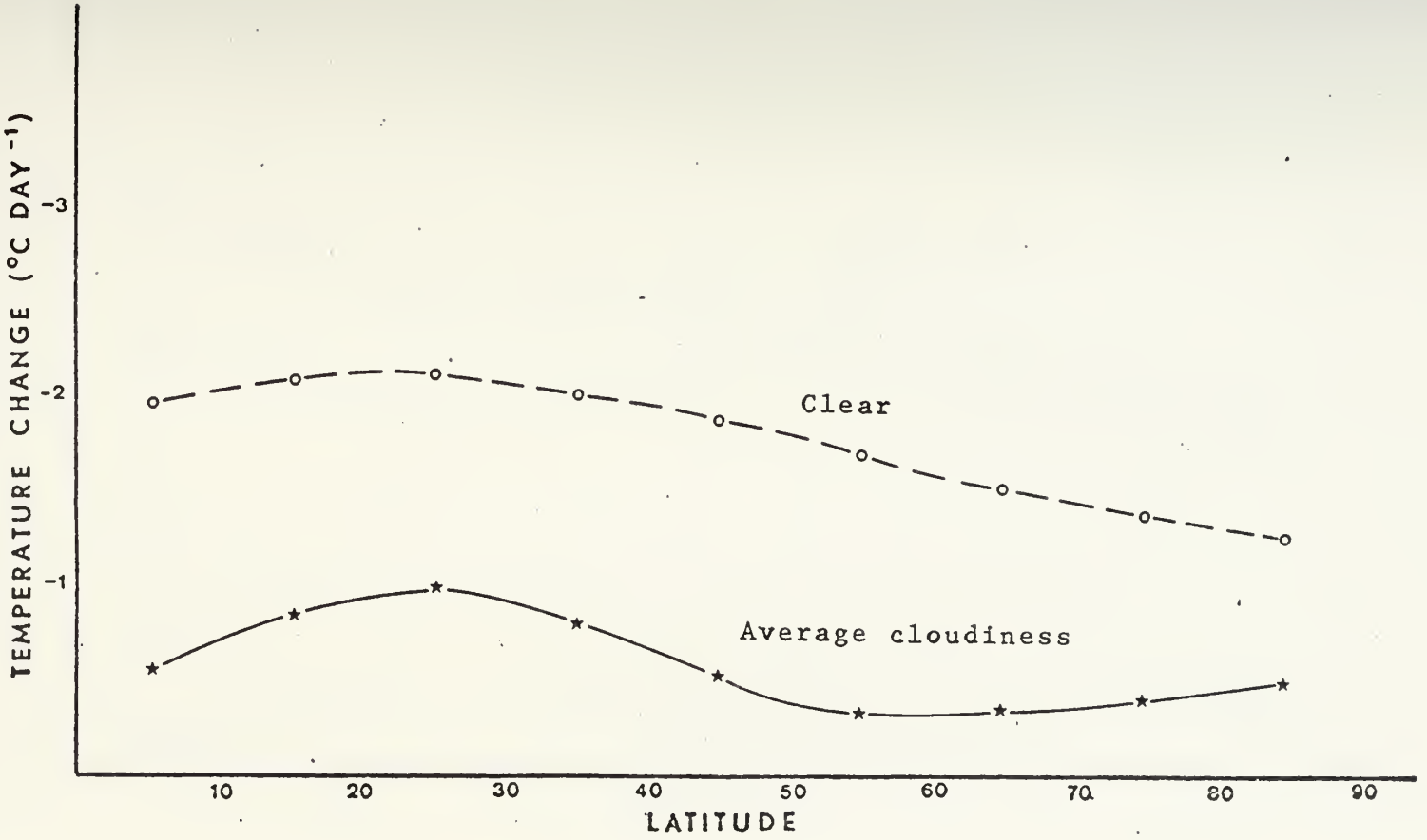

Figure 10. Mean annual infrared cooling rate in layer (6,10) with clear and average cloudy skies.

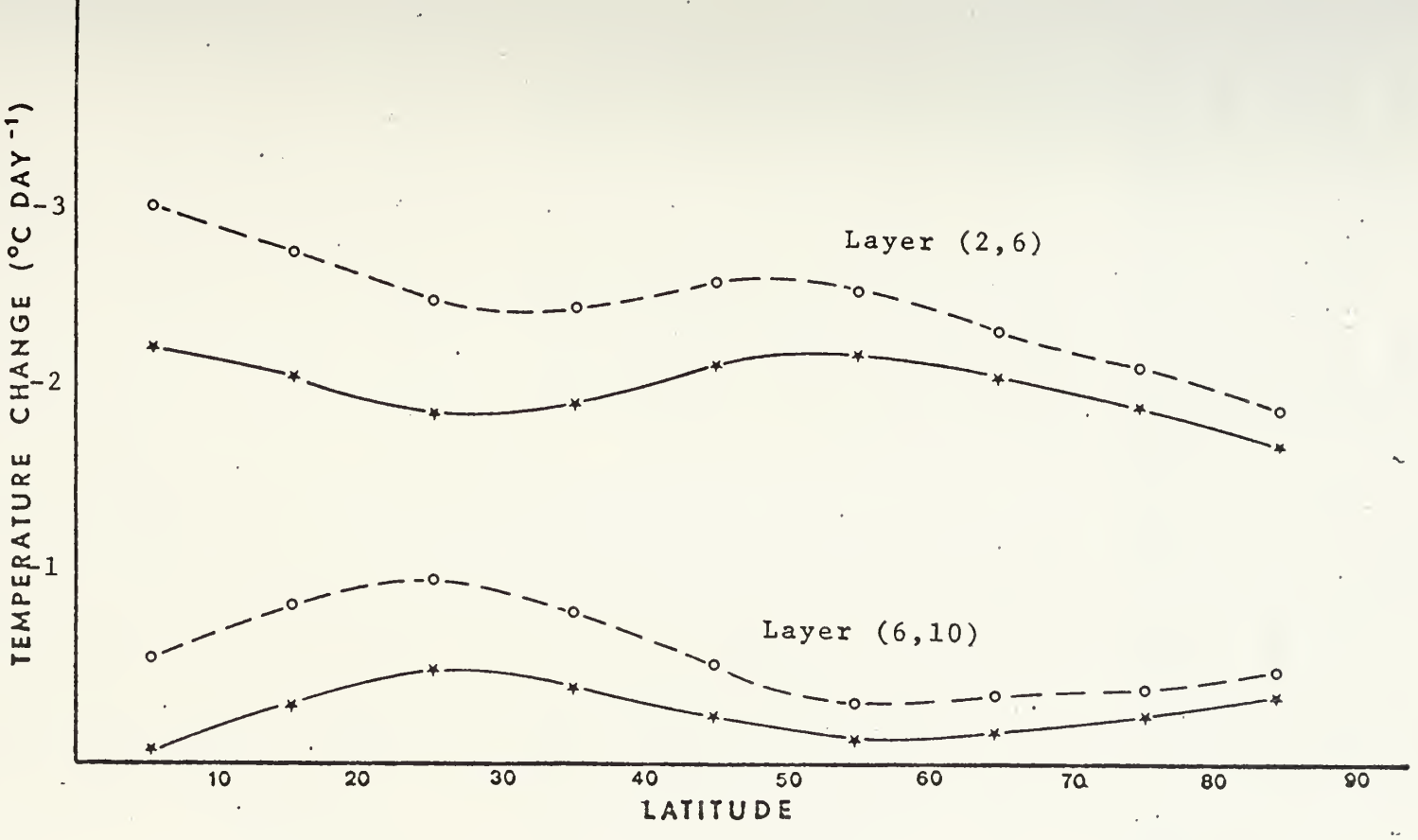

Figure 11. Comparison of mean annual atmospheric temperature change for infrared cooling and net radiation for layers (6,10) and (2,6).

solid curves represent the result of net radiative cooling (combined effects of long and short wave radiation) in the same layers. Atmospheric absorption clearly only modified the magnitude of radiative cooling while the shape of the curves was unchanged. By comparison of Figures 8 and 11, high correlations between net radiative temperature changes and total cloud cover may once again be noted.

VI. RADIATIVE BALANCE AT THE TROPOPAUSE

A radiative budget was calculated at the tropopause and compared to the results of Houghton (1954). Houghton made a comparison of the net incoming solar radiation at the tropopause with the outgoing long-wave flux. He determined that insofar as the earth-atmosphere combined system is concerned, a column at about 35°N latitude experiences a mean radiative energy balance. Corresponding latitude belts of the system located equatorward of latitude 35N have a mean annual radiative energy surplus. Those latitude bands poleward of 35°N latitude experience a mean annual radiative energy deficit. These mean annual radiative surpluses and deficits impose requirements for horizontal heat transfer rates across latitude walls in both air and ocean.

The net insolation at the tropopause (Q_o) is given by

$$Q_o = Q_I - Q_R \tag{70}$$

where Q_I is the incident insolation at the tropopause after a 4% reduction due to attenuation in the stratosphere. Q_R is the reflected insolation returned to space. The ratio of $Q_R/[1.04\ Q_I]$ is the measure of the earth atmosphere planetary albedo. Q_R is given by

$$Q_R = Q_I - Q_A - Q_{10} \tag{71}$$

where Q_A is the short wave radiation absorbed in the atmosphere and Q_{10} is the total short wave radiation absorbed at earth.

The resultant Q_R is a function of the Rayleigh back scattering, cloud reflectivity and surface albedo. The factors determining Rayleigh scattering were discussed in Section IV.

Treatment of cloud reflectivity was limited here by the use of a single cloud layer. A global average of about one-fourth of the incident solar radiation is reflected to space by clouds. In this model a single cloud albedo $R_c = 0.5$ was used. Sellers (1965) employed a range of albedos for differing cloud types. A similar treatment using various cloud types with various albedos was adopted by London. On a mean annual basis, 0.5 appears to be a good approximation for the hemispheric cloud reflectivity, but on an individual gridpoint basis the cloud albedos adopted in this study may be an oversimplification. Future testing in this area is envisioned for the NPS predictive model.

A single constant surface albedo of 0.14 was chosen after experimentation with the tropospheric energy balance. Budyko (1955) estimated the mean earth surface albedo as 0.14 while Katayama (1967) found a value of 0.13. But the albedo varies with the type of surface. The short-wave albedo is highest over fresh snow (90%) and is lowest over water and forests (approximately 5%). Since there are seasonal as well as annual variations in the extent of vegetation and snow cover, an attempt at strict evaluation

of ground albedo for these variations is at best difficult. Thus, for simplicity, a single mean ground albedo was employed.

The net outgoing long-wave radiation at the tropopause was given by F_2^* since the 0.2 sigma level was adopted as the mean height of the tropopause.

Therefore, the net radiative flux across the tropopause is given by

$$Q_N = Q_o - F_2^* \qquad (72)$$

Results for seasonal variations in the net flux across the tropopause are listed in Tables XII(a-d). The mean annual radiative input by latitude bands is listed in Table XII(e) along with the cosine-latitude weighting factors. The resulting mean Northern Hemisphere radiative budget is zero as anticipated, since it is assumed that the hemisphere is in annual radiative balance.

During the summer, the tropopause has a net radiative surplus throughout all latitude bands. As seen in Table XII(b), the incident insolation is largest during this season and far exceeds the small increase in net long wave radiation due to warmer summer temperatures. The opposite case is true for winter. Low insolation rates produced a negative radiative budget at all latitude bands except the 0-10° band. This particular latitude band has a positive radiative net surplus during the entire year. Spring and fall show transitions between the extremes of summer and winter.

TABLE XII(a). Net radiative budget (ly day^{-1}) at the tropopause with average cloud cover. (Spring)

Latitude	0-10	10-20	20-30	30-40	40-50	50-60	60-70	70-80	80-90
Q_I	884	896	889	848	784	702	604	503	468
Q_R	312	287	289	305	304	282	237	201	187
Q_o	572	609	600	543	480	420	367	302	281
F_2^*	488	510	499	449	410	378	344	313	304
Net Radiative Input	84	99	101	94	70	42	23	-11	-23

TABLE XII(b). Radiative budget (ly day^{-1}) at the tropopause with average cloud cover. (Summer)

Latitude	0-10	10-20	20-30	30-40	40-50	50-60	60-70	70-80	80-90
Q_I	867	922	952	965	948	916	882	888	908
Q_R	318	318	307	306	346	362	353	366	361
Q_o	549	504	645	649	602	554	529	522	547
F_2^*	491	506	511	494	461	420	395	370	366
Net Radiative Input	58	98	134	165	141	134	134	152	181

TABLE XII(c). Radiative budget (ly day^{-1}) at the tropopause with average cloud cover. (Fall)

Latitude	0-10	10-20	20-30	30-40	40-50	50-60	60-70	70-80	80-90
Q_I	844	783	696	593	473	339	195	64	0
Q_R	306	268	223	202	179	139	82	26	0
Q_o	538	515	473	391	294	200	113	38	0
F_2^*	478	501	504	478	422	379	343	319	308
Net Radiative Input	60	14	-31	-87	-128	-179	-230	-281	-308

TABLE XII(d). Radiative budget (ly day^{-1}) at the tropopause with average cloud cover. (Winter)

Latitude	0-10	10-20	20-30	30-40	40-50	50-60	60-70	70-80	80-90
Q_I	784	692	571	443	306	174	59	0	0
Q_R	266	207	178	158	120	71	24	0	0
Q_o	518	485	393	285	186	103	35	0	0
F_2^*	516	525	490	408	374	338	308	294	265
Net Radiative Input	2	-40	-97	-123	-188	-235	-273	-294	-265

TABLE XII(e). Mean annual radiative budget at the tropopause.

Latitude	0-10	10-20	20-30	30-40	40-50	50-60	60-70	70-80	80-90
Net Annual Radiative Input	51	42	27	12	-26	-59	-86	-108	-103
Cosine Weighting Factor	.9962	.9659	.9063	.8192	.7072	.5737	.4228	.2591	.0874
Annual Northern Hemisphere Rad. Balance	0.0								

Effects of variations in cloud cover on the computed net radiative input at the tropopause can be seen in Table XIII which lists spatial mean averages of the radiative quantities across the tropopause. It is seen that clouds exert an overall cooling effect in this model.

TABLE XIII. Spatial mean annual net radiative input at the tropopause (Northern Hemisphere).

	CL = 0	CL = 1.0	Average CL
Q_I	694	694	694
Q_R	130	360	244
Q_o	564	334	450
F_2^*	528	373	450
Net Tropopause Radiative Input	36	-39	0

VII. GLOBAL ALBEDO

The earth's global albedo results from the upward reflection by the ground, by clouds and by scattering by atmospheric molecules of solar radiation. Variations in computed planetary albedo are strongly dependent on total cloud cover. The distribution with latitude and season of global albedo is listed in Table XIV. There is a pronounced minimum in the subtropics, which is a region of minimum cloudiness. The minimum shifts equatorward during the winter and poleward during the summer, following movement of the ITCZ. The increased albedo in high latitudes during all seasons results from an increase in cloudiness with latitude up to about 60 to 70N.

Total global albedo when averaged over all latitudes and seasons is about 34 percent. The total global albedo shows little variation with season and agrees closely with London's results. Figure 12 shows a comparison between mean annual planetary albedo with latitude computed by London and the results of this study. Even though the spatially averaged annual global albedo of 34% agrees closely with London, there is disagreement in its distribution with latitude, a fact referred to in Section IV.

In tropical latitudes, London's global albedo was less than that computed in this study, while in the northern latitudes, his values exceeded those computed here. Since

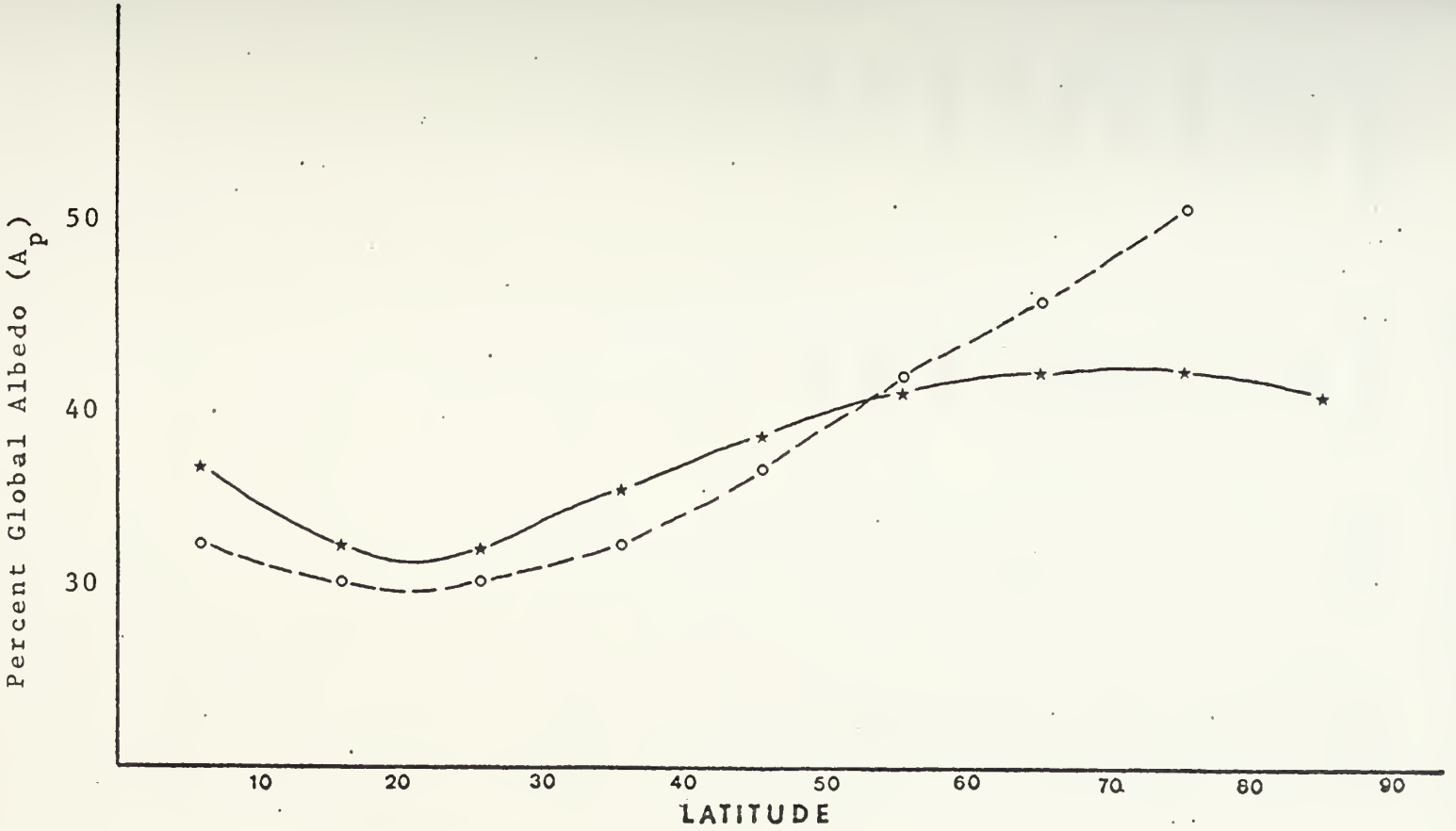

Figure 12. Comparison of mean annual global albedo distributions with latitude.

TABLE XIV. Seasonal distribution of planetary albedo with latitude (in percent of Q_I).

Latitude	Spring	Summer	Fall	Winter
0-10	35	37	36	34
10-20	32	35	34	30
20-30	32	32	32	31
30-40	36	32	34	36
40-50	39	37	38	39
50-60	40	40	41	41
60-70	39	40	42	40
70-80	40	41	41	-
80-90	40	40	-	-

identical total cloud cover amounts were used in both studies, the treatment of atmospheric and cloud albedos seem to be the major cause for this difference. The present study used a constant cloud albedo of $R_c = 0.5$ while London used varying cloud albedos associated with constituent cloud types after Haurwitz (1948). London thus used a multi-layer cloud model while this was not done here. Furthermore, the device of replacing the diffuse path length in clouds by an equivalent path 5/3 longer seems to give too short a path subject to cloud-reflecting processes at high latitudes and too long a path at low latitudes. This is important if cloud-reflectance is to be treated by Mie-scattering theory. Variations of surface reflectance with solar zenith angle also plays a secondary role in explaining the variations of A_p with latitude.

VIII. ATMOSPHERIC BUDGET

A simplified annual atmospheric heat budget for the Northern Hemisphere, along with seasonal distributions of radiative surpluses and deficits was constructed. The stratosphere was assumed to be in radiative equilibrium.

The atmosphere radiation balance is shown schematically below:

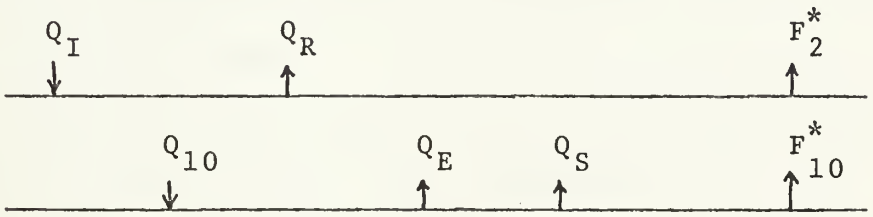

The net cooling contribution due to long wave radiation is given by

$$F_N = F_2^* - F_{10}^* \tag{73}$$

The effective insolation at the top of the troposphere is the total incident solar radiation minus the reflected insolation to space. The total atmospheric absorption is therefore

$$Q_A = (Q_I - Q_R) - Q_{10} \tag{74}$$

where Q_{10} is the short wave radiation absorbed at earth using a mean surface albedo, $\alpha_g = .14$. A final heating term consists of the latent heat of evaporation and sensible heat transfer rates across the earth-air interface and denoted by Q_H:

$$Q_H = Q_E + Q_S \tag{75}$$

The parameterization of Q_E and Q_S is detailed in Section IX. For each latitude band, the net atmospheric heating rate by the three mechanisms (insolation absorption, long-wave absorption, interface convection) is given by:

$$Q_{VA} = Q_H + Q_A - F_N \qquad (76)$$

The resulting atmospheric heating (cooling) rates in ly day^{-1} are summarized in Tables XV(a-d) for each latitude band and each of the four seasons, while Table XV(e) gives the annual mean, derived by averaging the four seasonal heating rates, as a function of latitude.

It is to be noted that Q_{VA} has been termed the "balance requirement" by Davis (1963), and represents the excess amount to be disposed of from a latitude belt by poleward flux-divergence of heat. Table XV(e) shows that the global annual average of this parameter (as calculated in this study) is zero.

Warming of the atmosphere by the absorption of solar radiation is less than the long-wave cooling rate. The net result is that the atmosphere is cooling radiatively at all latitudes at a rate of about 1.1°C day^{-1}. The compensating energy requirement for possible balance has been indicated by Equation (76) as arising by sensible and latent heat transfers across the earth surface.

With the addition of sensible and latent heat into each latitude band, Table XI(e) shows that latitude bands equatorward of 40N have a total energy surplus while latitude

bands poleward of 40N exhibit an energy deficit. While the mechanisms of horizontal transport are not specified in this study, the resultant globally-weighted values of Q_{VA} of Table XV(e) indicate a mean annual total heat balance in the atmosphere. The poleward redistribution required to effect this total heat balance is evidently brought about by general circulation processes, which were not considered in this study. For our purposes it suffices to show that the energy-generating aspects of the model proposed here is subject to an atmospheric balance.

TABLE XV(a). Atmospheric heating rates (ly day^{-1}), based upon climatological cloud cover. (Spring)

Latitude	0-10	10-20	20-30	30-40	40-50	50-60	60-70	70-80	80-90
$Q_0 - Q_R$	572	609	600	543	480	420	366	302	281
Q_{10}	451	484	487	450	405	361	317	264	248
Q_A	121	125	113	93	75	59	49	38	33
F_2	488	510	499	449	410	378	344	313	304
F_{10}	142	161	157	133	116	106	93	70	75
F_N	346	349	342	316	294	272	251	243	229
CL(%)	51	42	42	52	59	62	60	59	55
Q_H	304	390	284	245	175	155	110	68	25
Q_{VA}	79	166	55	24	-44	-58	-202	-235	-196

TABLE XV(b). Atmospheric heating rates (ly day^{-1}), based upon climatological cloud cover. (Summer)

Latitude	0-10	10-20	20-30	30-40	40-50	50-60	60-70	70-80	80-90
$Q_0 - Q_R$	549	604	645	659	602	554	530	522	547
Q_{10}	430	471	510	525	484	451	430	430	454
Q_A	119	133	135	134	118	103	100	92	93
F_2	491	506	511	494	461	420	395	370	366
F_{10}	145	146	157	145	118	103	100	83	82
F_N	346	360	354	349	343	317	295	287	284
CL(%)	54	49	42	41	55	63	66	69	64
Q_H	307	306	245	217	168	151	105	17	0
Q_{VA}	70	79	26	2	-57	-63	-195	-195	-191

TABLE XV(c). Atmospheric heating rates (ly day^{-1}), based upon climatological cloud cover. (Fall)

Latitude	0-10	10-20	20-30	30-40	40-50	50-60	60-70	70-80	80-90
$Q_0 - Q_R$	538	515	473	391	295	199	114	38	0
Q_{10}	424	404	374	315	241	166	95	31	0
Q_A	114	111	99	76	54	33	19	7	0
F_2	478	501	504	478	422	379	343	319	308
F_{10}	136	152	160	146	111	97	78	76	72
F_N	342	349	344	332	311	282	265	243	236
CL(%)	53	48	41	46	56	66	70	70	60
Q_H	277	363	290	301	192	181	120	68	25
Q_{VA}	49	25	45	45	-65	-68	-246	-236	-236

TABLE XV(d). Atmospheric heating rates (ly day^{-1}), based upon climatological cloud cover. (Winter)

Latitude	0-10	10-20	20-30	30-40	40-50	50-60	60-70	70-80	80-90
$Q_0 - Q_R$	518	485	393	285	186	103	35	0	0
Q_{10}	409	385	316	234	157	88	30	0	0
Q_A	109	100	77	51	29	15	5	0	0
F_2	516	525	490	408	374	338	308	294	265
F_{10}	161	180	166	126	101	83	68	81	90
F_N	355	345	324	282	273	255	248	213	175
CL(%)	47	36	38	50	59	63	58	47	40
Q_H	332	410	274	188	135	90	70	60	35
Q_{VA}	86	165	27	-43	-109	-150	-243	-213	-175

TABLE XV(e). Mean annual atmospheric heating rates (ly day^{-1}).

Latitude	0-10	10-20	20-30	30-40	40-50	50-60	60-70	70-80	80-90
Mean Annual Q_{VA} Balance	71	109	38	7	-69	-85	-120	-166	-178
Cosine Weighted Q_{VA} Balance	71	95	35	6	-49	-49	-50	-43	-16
Northern Hemisphere Balance		0							

IX. SURFACE HEAT TRANSFERS

The earth's surface heat balance was computed using evaporation and sensible heat transfers over the oceans as surface heat sinks. Heat transfer due to evaporation and sensible heat are more easily computed over ocean surfaces using climatological data available in the Pacific Ocean representative of the latitude belt as a whole. In effect, London's atmospheric soundings were used in association with data for ocean surface temperatures and surface winds taken from U. S. Weather Bureau's Atlas of Climatic Charts of the Oceans (1938). Continuity of sounding data with the oceanic reports was maintained by maintaining the same temperature lapse rate in the layer zero to 1 km.

The surface radiative budget is shown schematically below:

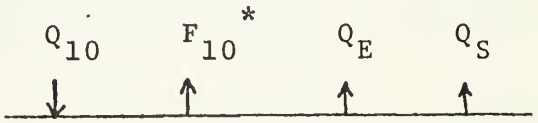

and may be stated symbolically by the equation:

$$Q_{10} - (F_{10}^* + Q_E + Q_S) = Q_{VO} \qquad (77)$$

Here Q_{VO} is the required oceanic heat transport divergence. The surface layer evaporation heat transfer rate was calculated after Langlois and Kwok (1969) using:

$$Q_E = L \rho_{10} C_D V_S (q_{sg} - q_x) \qquad (78)$$

with the constants:

$$L = 590 \text{ cal gram}^{-1}$$

$$\rho_{10} = 1.2 \times 10^{-3} \text{ gram cm}^{-3}$$

Also V_S is the climatological ocean surface wind speed incremented by 2.2 mps in order to account for the effect of gustiness upon evaporation [Langlois and Kwok (1969)]. A variable drag coefficient C_D proposed by Deacon and Webb (1962) for the case of neutral stability was employed:

$$C_D = (1.0 + 0.07\ V_S) \times 10^{-3} \tag{79}$$

At the ocean surface, the atmosphere was assumed to be saturated with respect to a plane water surface. The surface specific humidity, q_{sg}, was computed using the Clausius-Clapeyron equation:

$$q_{sg} = \frac{.622\ e^{(AE-BE/TG)}}{\pi - e^{(AE-BE/TG)}} \tag{80}$$

The specific humidity at the top of the constant flux surface layer, q_x, is given following the parameterization of the planetary boundary layer by Langlois and Kwok, by the formula:

$$q_x = \frac{kq_9 + (Z_9 - Z_{10})\ C_D\ V_S\ q_{sg}}{k + (Z_9 - Z_{10})\ C_D\ V_S} \tag{81}$$

with:

$$k = \frac{k^*}{1 + \dfrac{a^*(\theta_9 - \theta_S)}{Z_9 - Z_{10}}} \tag{82}$$

In (82), k^* and a^* are turbulent transfer coefficients whose values have been documented by Kaitala (1972).

Ice free oceans exist equatorward of 60N for all seasons. Therefore, air and sea temperature and wind data were required for only the first six latitude bands. Since London's atmospheric data was distributed at one-kilometer intervals, $(Z_9 - Z_{10})$ was taken as 1 km; also T_9 and q_9 are temperature and specific humidity at the one-km height. The first kilometer temperature lapse rate was computed using London's soundings. Air temperature at the ocean surface was assumed equal to the ocean surface temperature. The lapse rate was then applied to yield a new T_9 for use in (82). The new specific humidity q_9 at 1 km was generated using the relative humidity from London's data and the Clausius Clapeyron equation.

Sensible heat transfer rates equatorward of 60N were computed using Bowen ratio (r) values from Sellers (1965) and the formulation:

$$Q_S = r\, Q_E \tag{83}$$

Poleward of 60N, combined evaporation and sensible heating rates were taken from an assessment of many thousands of ship (and also of ice island) reports made by Vowinckel and Taylor (1964).

Tables XVI(a-d) contain the seasonal surface radiative balances, Q_{VO}, which is the oceanic heat transfer requirement by poleward flux-divergence. Seasonal variations can be compared against the annual mean values listed in Table XVI(e).

The physical meaning of a negative Q_{VO} value for a latitude belt in the tropics (with positive values in northerly belts) is that a flux-convergence (divergence) of sensible heat due to ocean currents is needed to maintain a long-term balance.

TABLE XVI(a). Surface heating rates (ly day^{-1}). (Spring)

Latitude	0-10	10-20	20-30	30-40	40-50	50-60	60-70	70-80	80-90
Q_{10}	451	484	487	450	405	361	317	264	248
F_{10}^{*}	142	161	157	133	116	106	93	70	75
$Q_{10} - F_{10}^{*}$	309	323	330	317	289	255	224	194	173
Q_E	290	368	261	213	138	110	110	68	25
Q_S	14	22	23	32	37	45			
Q_{VO}	5	-67	46	72	114	100	114	126	148

TABLE XVI(b). Surface heating rates (ly day^{-1}). (Summer)

Latitude	0-10	10-20	20-30	30-40	40-50	50-60	60-70	70-80	80-90
Q_{10}	430	471	510	525	484	451	430	430	454
F_{10}^{*}	145	146	157	145	118	103	100	83	82
$Q_{10} - F_{10}^{*}$	285	325	353	380	366	348	330	347	372
Q_E	293	289	227	189	133	107	105	17	0
Q_S	14	17	18	28	35	44			
Q_{VO}	-22	19	108	163	198	197	225	330	372

TABLE XVI(c). Surface heating rates (ly day^{-1}). (Fall)

Latitude	0-10	10-20	20-30	30-40	40-50	50-60	60-70	70-80	80-90
Q_{10}	424	404	374	315	241	166	95	31	0
F_{10}^*	136	152	160	146	111	97	78	76	72
$Q_{10} - F_{10}^*$	288	252	214	169	130	69	17	-45	-72
Q_E	264	344	267	261	152	128	120	68	25
Q_S	13	21	23	40	40	53			
Q_{VO}	11	-111	-76	-132	-62	-112	-103	-113	-97

TABLE XVI(d). Surface heating rates (ly day^{-1}). (Winter)

Latitude	0-10	10-20	20-30	30-40	40-50	50-60	60-70	70-80	80-90
Q_{10}	409	385	316	234	157	88	30	0	0
F_{10}^{*}	161	180	166	126	101	83	68	81	90
$Q_{10} - F_{10}^{*}$	248	205	150	108	56	5	-38	-81	-90
Q_E	316	387	252	163	107	64	70	60	35
Q_S	16	23	22	25	28	26			
Q_{VO}	-74	-205	-124	-80	-79	-85	-108	-141	-125

TABLE XVI(e). Mean annual surface heating budget estimated by the NPS model (ly day^{-1}).

Latitude	0-10	10-20	20-30	30-40	40-50	50-60	60-70	70-80	80-90
Mean Q_{VO}	-20	-91	-12	3	43	25	32	51	50
Cosine Weighting Factor	.9962	.9659	.9063	.8192	.7072	.5737	.4228	.2591	.0874
Weighted Q_{VO}	-20	-88	-11	2	31	13	14	13	4
Northern Hemisphere Annual Average	-42								

X. CONCLUSION

With the use of mean seasonal atmospheric data, a proposed radiation-heating model for the Naval Postgraduate School primitive-equation predictive system was evaluated. The model proved readily adaptable to computerization.

The time and space averaged radiational quantities showed rather good agreement as a whole when compared with the results of other researchers. Minor difference in the comparisons can generally be ascribed to the treatment of global albedo, and the assumption of but a single cloud layer. While the average global albedo determined in this study is typical of usual values quoted, namely 34%, the meridional distribution of global albedo was more nearly uniform with respect to latitude than would have resulted if the mean value had been based upon hourly computations for the months involved. This result led to a lower than normal value of solar radiation absorbed within the earth's surface in low latitudes and a larger than typical value absorbed in high latitudes.

Of the three heat budgets discussed, results compatible with Houghton (1954) and Davis (1963) respectively, were demonstrated for the earth-atmosphere system and for the magnitude and direction of the required total heat flow. Similar tests were also applied to the ocean surface where the distribution of surface heat-flux divergence was

opposite to that expected (e.g. Budyko (1955)), the results of the surface heat budget were somewhat biased by the averaging involved in the derivation of the global albedo, as explained previously.

Finally, while the radiation package has proven generally adaptable to a general circulation predictive model, further refinements are anticipated in the treatment of cloud cover. A two-layer cloud model for the treatment of middle and low-level clouds has been suggested. These two cloud types would have different short-wave flux reflection and absorption characteristics and would lead to a more accurate determination of global albedo.

APPENDIX A

Evaluation of the final temperature-dependent flux integral $\int \bar{\epsilon}\,(u_o, T_1)\,dB$ for a variety of final temperature values (T_1) and final scaled water-vapor values (ly day^{-1})

Scaled Water Vapor	190°	195°	200°	205°	210°	215°	220°
0.0001	26.98	28.53	30.12	31.76	33.45	35.19	36.97
0.0005	42.62	45.36	48.19	51.13	54.16	57.30	60.55
0.001	50.84	54.25	57.80	61.48	65.30	69.26	73.36
0.002	59.89	64.09	68.46	73.01	77.75	82.66	87.78
0.004	69.65	74.74	80.05	85.60	91.38	97.41	103.68
0.006	75.63	81.29	87.20	93.39	99.85	106.59	113.61
0.008	79.97	86.05	92.41	99.08	106.04	113.32	120.91
0.01	83.37	89.79	96.52	103.57	110.94	118.64	126.69
0.015	89.63	96.68	104.09	111.86	120.00	128.53	137.44
0.02	94.09	101.61	109.52	117.83	126.54	135.67	145.22
0.03	100.38	108.57	117.21	126.30	135.83	145.84	156.34
0.04	104.80	113.49	122.65	132.30	142.45	153.11	164.29
0.06	110.94	120.33	130.25	140.71	151.73	163.33	175.51
0.08	115.20	125.09	135.56	146.60	158.25	170.52	183.42
0.1	118.42	128.71	139.60	151.10	163.24	176.04	189.51
0.15	124.08	135.08	146.73	159.07	172.11	185.87	200.37
0.2	127.90	139.40	151.59	164.52	178.19	192.64	207.89
0.3	132.96	145.15	158.10	171.84	186.40	201.81	218.10
0.4	136.30	148.96	162.43	176.74	191.92	208.00	225.01
0.5	138.72	151.74	165.61	180.35	196.00	212.60	230.16
0.6	140.59	153.89	168.07	183.16	199.19	216.20	234.22
0.8	143.31	157.05	171.72	187.34	203.95	221.59	240.30
1.0	145.22	159.29	174.32	190.33	297.38	225.50	244.73
1.5	148.23	162.86	178.50	195.20	213.00	231.96	252.10
2.0	149.99	164.97	181.02	198.17	216.48	235.98	256.73
2.5	151.12	166.36	182.70	200.18	218.85	238.76	259.97
3.0	151.89	167.33	183.90	201.63	220.59	240.81	262.36
4.0	152.82	168.55	185.44	203.55	222.92	243.61	265.68
5.0	153.29	169.23	186.35	204.72	224.38	245.41	267.86
6.0	153.53	169.61	186.90	205.46	225.35	246.63	269.40
8.0	153.59	169.88	187.41	206.24	226.45	248.09	271.23
10.0	153.40	169.81	187.50	206.51	226.94	248.82	272.25
15.0	152.49	169.08	186.98	206.26	227.00	249.26	273.11
25.0	150.35	167.04	185.09	204.58	225.57	248.14	272.38
30.0	149.32	166.02	184.09	203.61	224.66	247.30	271.63

APPENDIX B

Water-vapor equivalent u_c for droplet absorption in relation to the pressure-scaled water-vapor absorber mass u(4,8) (in the sounding layer (4,8)). Case $u_c(1)$ corresponds to low latitude water-drop absorptivity; $u_c(2)$ to mid-latitude absorptivity; $u_c(3)$ to high latitude absorptivity.

u(4,8)	$u_c(1)$	$u_c(2)$	$u_c(3)$
0.01	0.14170	0.05118	0.00740
0.02	0.18936	0.97292	0.01155
0.05	0.28886	0.12003	0.02103
0.10	0.40852	0.17851	0.03329
0.15	0.50529	0.22673	0.04365
0.20	0.56995	0.26939	0.05294
0.30	0.73785	0.34473	0.96955
0.50	0.98617	0.47287	0.09826
0.80	1.29740	0.63548	0.13520
1.00	1.48119	0.73226	0.15739
1.20	1.65219	0.82271	0.17822
1.40	1.81232	0.90822	0.19800
1.60	1.96648	0.98974	0.21691
1.80	2.11306	1.06793	0.23510
2.00	2.25403	1.14331	0.25267
2.20	2.39016	1.21623	0.26970
2.40	2.52206	1.28699	0.28626
2.60	2.65022	1.35584	0.30240
2.80	2.77499	1.42297	0.31816
3.00	2.89675	1.48854	0.33357

APPENDIX C

The distribution of relative humidity and total optical mass (to the tropopause) u(gm cm^{-2})(from London, 1957).

April

Lat.°N	0-10		10-20		20-30		30-40		40-50		50-60		60-70		70-80		80-90	
Height (km)	R.H.	u	R.H.	u	R.H.	u	R.H.	u	R.H.	u	R.H.	u	R.H.	u	R.H.	u	R.H.	u
Surface	80	4.622	71	4.031	62	2.874	67	1.918	70	1.291	76	.806	81	.466	83	.299	80	.191
1	70	3.037	60	2.646	54	1.828	56	1.197	61	.793	64	.488	65	.291	66	.213	59	.139
2	62	1.909	51	1.489	45	1.096	47	.709	54	.456	57	.278	59	.173	58	.138	53	.0956
3	55	1.129	45	.858	40	.636	42	.398	48	.249	52	.150	55	.0938	54	.0733	49	.0585
4	49	.678	41	.487	36	.348	39	.213	45	.126	49	.0767	52	.0469	51	.0351	47	.0325
5	45	.398	37	.260	35	.137	36	.103	42	.0619	47	.0386	49	.0234	49	.0201	45	.0178
6	42	.217	36	.133	34	.0989	35	.0542	42	.0295	46	.0193	47	.0127	47	.0116	45	.0105
7	41	.118	35	.0682	34	.0507	35	.0270	42	.0155	45	.0101	45	.0071	46	.0068	45	.0062
8	42	.0647	35	.0323	34	.0237	37	.0144	41	.0083	45	.0058	45	.0039	46	.0038	46	.0035
9	45	.0341	37	.0224	36	.0126	40	.0076	42	.0046	45	.0035	45	.0020	47	.0018	48	.0015
10	49	.0163	40	.0112	40	.0066	43	.0043	44	.0026	47	.0019	47	.0007				
11	55	.0079	45	.0057	44	.0033	47	.0025	47	.0015	48	.0007						
12	60	.0034	51	.0027	50	.0018	52	.0014	51	.0006								
13	66	.0014	57	.0013	56	.0009	57	.0006										
14	72	.0005	65	.0006	64	.0004	63	.0001										
15	80	.0002	74	.0002	71	.0001												
16	86	.0001																
Tropopause	95		85		75		65		55		50		50		50		50	
Stratosphere		.0011		.0011		.0017		.0030		.0070		.0164		.0303		.0425		.0456

Summer

Lat. °N	0-10		10-20		20-30		30-40		40-50		50-60		60-70		70-80		80-90	
Height (km)	R.H.	M	R.H.	M	R.H.	M	R.H.	M	R.H.	M	R.H.	M	R.H.	M	R.H.	M	R.H.	M
Surface	84	5.233	77	5.093	72	4.196	72	3.420	74	2.701	76	2.048	78	1.646	80	1.192	80	1.014
1	76	3.215	70	3.166	62	2.599	60	2.064	64	1.630	70	1.261	72	.994	72	.742	73	.655
2	70	2.042	64	1.985	56	1.629	52	1.262	56	.985	63	.750	66	.590	66	.460	66	.428
3	63	1.256	59	1.226	50	.999	45	.769	50	.584	56	.430	60	.333	60	.262	60	.254
4	53	.715	54	.709	46	.579	42	.441	44	.326	50	.235	55	.180	56	.142	54	.107
5	55	.401	50	.397	42	.322	39	.245	40	.176	46	.126	51	.0974	51	.0759	49	.0538
6	52	.217	46	.206	40	.167	37	.129	39	.0946	44	.0633	48	.0509	50	.0388	43	.0271
7	48	.108	42	.0975	38	.0852	36	.0645	39	.0485	44	.0397	48	.0266	50	.0200	49	.0138
8	47	.0543	40	.0459	36	.0417	36	.0326	40	.0253	45	.0213	48	.0138	52	.0084	51	.0064
9	46	.0282	38	.0229	35	.0211	36	.0171	42	.0144	46	.0119	50	.0073	53	.0034	54	.0021
10	46	.0149	38	.0115	36	.0102	38	.0090	44	.0088	50	.0079	53	.0041	58	.0006		
11	49	.0072	41	.0055	39	.0047	40	.0046	46	.0054	52	.0053	57	.0014				
12	53	.0035	46	.0026	41	.0021	44	.0026	50	.0033	56	.0028						
13	59	.0017	52	.0011	48	.0011	48	.0015	52	.0020	58	.0007						
14	66	.0007	60	.0005	56	.0006	54	.0008	56	.0009								
15	74	.0003	68	.0002	62	.0003	60	.0003	59									
16	84	.0001	78	.0001	72	.0001	69											
Tropopause	90		88		78		68		60		60		60		60		60	
Stratosphere		.0013		.0017		.0031		.0053		.0107		.0243		.0439		.0648		.0910

October

Lat. °N	0-10		10-20		20-30		30-40		40-50		50-60		60-70		70-80		80-90	
Height (km)	R.H.	u	R.H.	u	R.H.	u	R.H.	u	R.H.	u	R.H.	u	R.H.	u	R.H.	u	R.H.	u
Surface	80	4.888	75	4.624	69	3.746	67	2.620	74	1.670	81	1.066	86	.646	85	.501	86	.306
1	71	3.261	66	2.969	60	2.380	57	1.663	65	1.049	70	.646	74	.401	72	.295	68	.204
2	64	2.094	59	1.838	52	1.459	50	.988	55	.629	60	.374	65	.235	64	.173	59	.123
3	58	1.289	53	1.093	45	.788	43	.582	48	.349	56	.202	58	.133	59	.0911	55	.0631
4	55	.760	49	.617	41	.441	39	.325	44	.192	49	.105	54	.0688	56	.0470	52	.0355
5	52	.419	45	.332	37	.240	36	.172	41	.101	47	.0540	52	.0351	54	.0269	51	.0200
6	50	.232	42	.180	35	.135	35	.0978	40	.0545	45	.0281	50	.0184	52	.0133	52	.0115
7	48	.127	39	.0974	35	.0728	36	.0532	41	.0287	45	.0149	50	.0092	52	.0078	51	.0067
8	47	.0674	38	.0501	36	.0392	38	.0279	43	.0144	47	.0081	50	.0050	52	.0041	52	.0032
9	48	.0340	38	.0250	38	.0202	42	.0137	46	.0070	49	.0047	52	.0024	52	.0017	56	.0009
10	51	.0162	40	.0125	39	.0094	46	.0065	49	.0038	55	.0026	52	.0007				
11	55	.0072	45	.0057	46	.0043	49	.0033	52	.0019	57	.0010						
12	61	.0030	52	.0024	51	.0021	54	.0016	56	.0008								
13	67	.0011	60	.0010	57	.0011	58	.0007										
14	72	.0004	68	.0004	65	.0005	63	.0001										
15	80	.0001	76	.0001	72	.0001												
16																		
Tropopause	90		85		75		65		60		60		60		60		60	
Stratosphere		.0011		.0011		.0014		.0041		.0070		.0139		.0272		.0425		.0455

Winter

Lat. °N	0-10		10-20		20-30		30-40		40-50		50-60		60-70		70-80		80-90	
Height (ku)	R.H.	u	R.H.	u	R.H.	u	R.H.	u	R.H.	u	R.H.	u	R.H.	u	R.H.	u	R.H.	u
Surface	82	4.443	74	3.776	74	2.379	76	1.556	78	.847	82	.468	81	.248	76	.137	69	.0795
1	68	2.753	64	2.268	59	1.398	62	.967	69	.526	72	.300	70	.175	68	.0982	60	.0690
2	58	1.685	54	1.207	48	.796	52	.577	60	.307	64	.180	62	.113	62	.0722	55	.0491
3	50	1.026	41	.709	40	.450	44	.338	52	.166	56	.0982	58	.0632	58	.0414	52	.0291
4	44	.627	38	.426	36	.257	40	.179	48	.0873	53	.0521	56	.0333	54	.0221	50	.0152
5	40	.370	34	.262	32	.146	38	.0846	46	.0464	50	.0283	52	.0180	52	.0121	50	.0083
6	38	.209	32	.146	30	.0839	36	.0457	44	.0250	50	.0153	51	.0100	50	.0069	50	.0048
7	36	.113	31	.0714	32	.0489	38	.0244	46	.0142	50	.0085	51	.0056	50	.0040	50	.0028
8	35	.0592	32	.0383	35	.0284	41	.0131	48	.0080	50	.0045	50	.0029	50	.0020	50	.0012
9	34	.0289	33	.0195	38	.0146	44	.0074	49	.0045	50	.0023	50	.0012	50	.0006		
10	36	.0145	36	.0098	42	.0061	48	.0043	52	.0027	52	.0009	50	.0001				
11	41	.0071	41	.0049	47	.0033	52	.0027	56	.0016								
12	47	.0033	48	.0023	52	.0017	57	.0016	60	.0006								
13	55	.0015	56	.0011	60	.0009	63	.0008										
14	65	.0006	66	.0005	66	.0005	69	.0003										
15	75	.0002	75	.0002	74	.0002												
16																		
Tropopause	90		90		82		72		62		62		52		50		50	
Stratosphere		.0006		.0008		.0013		.0038		.0086		.0110		.0103		.0108		.0137

APPENDIX D

The distribution of average temperature and pressure (from London, 1957).

April

Ht(km) Stn	T(°C)	p(mb)	0-10°N T(°C)	p(mb)	10-20°N T(°C)	p(mb)	20-30°N T(°C)	p(mb)	30-40°N T(°C)	p(mb)	40-50°N T(°C)	p(mb)	50-60°N T(°C)	p(mb)	60-70°N T(°C)	p(mb)	70-80°N T(°C)	p(mb)	80-90°N T(°C)	p(mb)
	26.2	1009	26.9	1013	23.1	1016	15.8	1017	8.7	1016	1.5	1014	- 7.3	1014	-16.2	1019	-21.1	1020		
1	22.2	905	22.4	908	19.0	908	11.8	906	4.5	900	- 2.6	898	- 9.8	894	-16.4	900	-21.3	898		
2	17.0	806	17.2	804	14.1	804	7.1	800	- 0.2	792	- 7.1	787	-13.6	784	-17.9	783	-22.0	784		
3	11.6	710	11.1	709	8.4	709	1.8	703	- 5.7	695	-12.4	687	-17.9	682	-21.2	680	-23.8	678		
4	5.7	630	5.4	627	2.3	622	- 4.3	618	-11.4	606	-18.2	599	-24.1	592	-27.0	587	-28.2	586		
5	0.0	557	- 1.2	552	- 4.4	548	-10.7	542	-17.9	530	-25.0	522	-31.0	514	-33.2	508	-34.6	507		
6	- 6.0	487	- 7.8	486	-11.4	484	-17.9	475	-25.1	465	-31.8	454	-37.2	448	-39.2	443	-40.0	440		
7	-12.1	428	-14.6	432	-19.0	424	-25.8	416	-32.9	410	-39.0	394	-42.6	388	-43.6	383	-44.2	380		
8	-18.8	378	-21.7	381	-26.3	365	-33.5	364	-39.9	358	-45.1	342	-47.1	332	-47.0	330	-47.6	328		
9	-25.8	332	-28.6	333	-33.7	322	-40.2	314	-46.2	308	-49.8	295	-50.6	286	-49.5	286	-50.0	282		
10	-33.0	288	-35.7	283	-40.6	281	-46.6	273	-51.2	263	-53.1	255	-52.9	249						
11	-40.6	252	-42.7	250	-47.5	242	-51.9	235	-54.7	227	-53.7	220								
12	-48.2	216	-49.8	214	-53.8	210	-56.6	201	-56.8	194										
13	-56.0	185	-56.9	182	-59.4	178	-60.5	172												
14	-63.8	154	-63.0	155	-65.2	150	-64.0	144												
15	-72.3	132	-69.2	130	-69.1	126														
16	-75.0	112	-74.6	111																
Stratosphere	-73.0	48	-71.6	52	-69.6	50	-65.8	50	-59.6	64	-53.2	70	-48.3	76	-45.6	80	-45.0	80		

Summer

	T(°C)	p(mb)	T(°C)	p(mb)	T(°C)	p(mb)	T(°C)	p(mb)	T(°C)	p(mb)	T(°C)	p(mb)	T(°C)	p(mb)	T(°C)	p(mb)
	0-10°N		10-20°N		20-30°N		30-40°N		40-50°N		50-60°N		60-70°N		70-80°N		70-90°N	
Sfc	27.3	1011	27.9	1011	26.9	1012	23.2	1014	18.3	1013	13.3	1011	9.6	1011	3.4	1014	0.4	1013
1	21.6	895	23.1	892	22.4	895	19.1	891	14.5	889	9.5	888	5.5	887	0.0	887	- 2.4	885
2	16.1	795	17.8	795	17.1	795	14.8	792	10.0	790	4.8	787	0.6	782	- 3.5	782	- 5.4	781
3	10.4	707	12.2	710	11.5	710	9.4	708	4.7	704	- 0.8	698	- 4.7	694	- 7.0	690	- 8.2	690
4	4.9	623	6.1	628	5.5	629	3.2	627	1.1	621	- 6.6	615	-10.8	610	-13.3	609	-15.2	609
5	- 0.9	550	0.0	555	- 0.6	554	- 3.1	553	- 7.7	545	-12.8	540	-17.0	535	-19.8	534	-22.5	532
6	- 7.3	485	- 6.1	487	- 6.6	487	- 9.4	485	-14.1	479	-18.8	470	-23.3	465	-26.3	461	-29.5	459
7	-14.1	424	-13.0	425	-13.6	429	-16.4	424	-20.9	416	-25.6	409	-29.5	404	-31.9	401	-34.8	398
8	-20.9	371	-20.0	370	-20.7	376	-23.4	371	-28.1	362	-32.4	355	-35.5	350	-37.8	345	-40.3	344
9	-27.7	326	-26.9	326	-27.8	330	-30.6	325	-34.9	318	-39.2	309	-41.8	304	-43.5	299	-45.5	298
10	-34.4	286	-33.9	287	-34.7	287	-37.8	284	-42.2	278	-46.0	271	-48.0	266	-49.6	261		
11	-41.2	247	-41.5	250	-42.4	248	-44.2	244	-46.5	239	-47.6	233						
12	-47.9	212	-48.8	216	-50.1	213	-50.8	212	-50.7	206	-49.3	200						
13	-54.9	181	-56.6	183	-58.0	183	-57.4	180	-55.3	176								
14	-61.5	153	-62.7	157	-62.6	156	-60.4	154	-56.3	148								
15	-68.5	130	-69.1	132	-67.3	133	-63.1	131										
16	-75.1	110	-75.7	111	-71.8	112												
Strato.	-71.3	41	-69.5	40	-66.7	43	-61.7	48	-56.8	55	-50.3	66	-45.4	77	-42.1	85	-39.?	87

October

Ht (km)	T(°C)	p(mb)	T(°C)	p(mb)	T(°C)	p(mb)	T(°C)	p(mb)	T(°C)	p(mb)	T(°C)	p(mb)	T(°C)	p(mb)	T(°C)	p(mb)	T(°C)	p(mb)
	0-10°N		10-20°N		20-30°N		30-40°N		40-50°N		50-60°N		60-70°N		70-80°N		80-90°N	
Sfc	26.2	1011	27.7	1012	25.5	1016	20.1	1018	10.7	1017	3.9	1013	- 4.4	1011	- 7.4	1013	-14.8	1015
1	21.8	904	22.8	904	21.2	906	15.8	906	7.7	902	0.2	896	- 7.2	890	- 0.8	890	-15.4	894
2	17.2	803	17.6	803	15.8	804	11.0	802	3.4	800	- 4.4	790	-11.0	780	-13.6	782	-17.2	780
3	12.0	710	11.8	710	9.6	710	5.3	708	- 2.3	700	- 9.7	690	-15.7	682	-18.9	680	-20.0	679
4	6.2	626	5.8	625	3.4	624	- 0.2	620	- 7.8	614	-15.6	602	-21.2	590	-26.2	590	-26.2	586
5	0.0	550	- 0.6	550	- 3.0	548	- 6.4	542	-14.0	536	-21.8	524	-27.4	512	-32.8	514	-33.8	510
6	- 6.8	487	- 7.4	487	- 8.6	486	-13.1	481	-20.5	471	-27.9	459	-34.2	449	-38.3	446	-40.0	445
7	-13.0	430	-13.6	430	-15.6	429	-19.2	423	-26.8	412	-35.2	401	-40.0	390	-42.8	390	-44.4	388
8	-19.5	378	-20.2	376	-22.4	378	-26.2	372	-34.0	358	-41.8	346	-45.4	340	-46.4	336	-47.4	333
9	-26.2	330	-27.0	328	-29.2	331	-33.4	324	-41.2	308	-47.2	300	-49.5	292	-49.1	288	-49.4	287
10	-33.0	287	-33.6	287	-36.6	285	-42.1	279	-47.8	269	-51.3	259	-51.9	252				
11	-41.0	248	-41.4	248	-45.0	244	-48.2	240	-53.0	230	-53.2	222						
12	-49.6	213	-49.4	214	-52.2	210	-54.6	206	-56.8	198								
13	-57.8	183	-57.9	183	-58.4	181	-59.4	176										
14	-64.8	156	-65.8	156	-64.2	152	-63.6	148										
15	-71.4	130	-71.6	130	-67.0	128												
16	-76.0	111																
Stratosphere	-72.8	52	-72.6	56	-71.2	60	-63.6	62	-58.9	64	-54.4	70	-49.1	76	-45.5	82	-45.0	84

Winter

	T(°C)	p(mb)	T(°C)	p(mb)	T(°C)	p(mb)	T(°C)	p(mb)	T(°C)	p(mb)	T(°C)	p(mb)	T(°C)	p(mb)	T(°C)	p(mb)	T(°C)	p(mb)
	0-10°N		10-20°N		20-30°N		30-40°N		40-50°N		50-60°N		60-70°N		70-80°N		80-90°N	
Sfc	27.3	1011	24.7	1014	19.4	1018	10.5	1019	0.4	1017	- 8.5	1015	-18.9	1014	-25.1	1016	-30.2	1017
1	21.9	905	19.1	904	15.3	907	7.0	906	- 2.8	901	-10.7	894	-18.6	892	-24.6	891	-29.6	891
2	16.4	806	13.6	805	9.5	805	2.7	801	- 6.4	793	-13.8	786	-20.0	780	-25.0	778	-29.4	777
3	11.3	715	8.3	713	3.9	712	- 2.4	706	-10.8	695	-17.7	686	-22.7	679	-26.9	675	-29.3	672
4	5.9	635	2.7	632	- 2.1	630	- 8.9	622	-17.4	611	-23.8	600	-28.9	593	-32.9	588	-35.7	585
5	0.3	563	- 4.1	559	- 8.4	555	-15.3	547	-23.7	534	-30.0	524	-35.0	516	-38.8	511	-42.0	506
6	- 5.0	495	- 8.8	493	-14.1	487	-21.4	477	-30.0	465	-36.1	454	-41.0	447	-44.4	441	-47.6	437
7	-11.3	436	-15.2	432	-21.0	427	-28.5	417	-36.0	405	-41.2	394	-45.0	384	-47.7	380	-50.0	378
8	-17.6	382	-21.7	378	-27.7	372	-35.5	362	-41.9	351	-46.3	339	-49.1	331	-50.8	328	-52.2	325
9	-24.2	332	-28.4	329	-34.5	323	-42.5	314	-47.8	301	-51.0	292	-52.9	283	-54.0	280		
10	-32.2	290	-36.0	285	-42.2	279	-48.7	269	-53.5	258	-56.0	248						
11	-39.5	250	-42.9	247	-48.9	242	-53.1	231	-55.4	222								
12	-47.2	215	-51.0	213	-55.3	207	-57.1	198	-57.2	189								
13	-54.3	185	-57.5	182	-60.8	176	-60.4	167										
14	-61.4	159	-64.1	156	-65.4	150	-62.6	144										
15	-63.0	133	-69.7	132	-69.0	127												
16	-74.8	113	-74.5	110														
Strato	-73.0	42	-73.9	46	-70.0	47	-66.5	53	-61.9	63	-56.9	70	-54.8	74	-53.6	76	-52.5	79

LIST OF REFERENCES

1. Arakawa, A., 1972: Design of the UCLA general circulation model. Numerical Simulation of Weather and Climate Tech. Rpt. No. 7, Department of Meteorology, University of California.

2. Arakawa, A., A. Katayama and Y. Mintz, 1968: Numerical simulation of the general circulation of the atmosphere. Proceedings of the WMO/IUGG Symposium on Numerical Weather Prediction, Tokyo, 1968, pp. IV-7 to IV-8-12.

3. Brunt, D., 1939: Physical and dynamical meteorology, Cambridge University, London, 428 pp.

4. Budyko, M. I., 1955: The Heat Balance of the Earth's Surface, Leningrad, Central Geophysical Observatory, 255 pp.

5. Coulson, K. L., 1959: Radiative flux from the top of a Rayleigh atmosphere. Ph.D. dissertation, Department of Meteorology, University of California, Los Angeles, pp. 60.

6. Davis, P. A., 1963: An Analysis of the Atmosphere Heat Budget. Journal of the Atmospheric Sciences, vol.20, no. 1, pp. 5-21.

7. Deardorff, J. W., 1966: The counter-gradient flux in the lower atmosphere and in the laboratory. Journal of the Atmospheric Sciences, vol. 23, no. 5, pp. 503-506.

8. Elsasser, W. M., 1937: On some properties of the water vapor spectrum and their relations to atmospheric radiation. Monthly Weather Review, vol. 65, no. 3, pp. 323-326.

9. Gates, W. L., E. S. Batten, A. B. Kahle and A. B. Nelson, 1971: A documentation of the Mintz-Arakawa two-level atmospheric circulation model. Advance Research Projects Agency Report No. R-877-ARPA, Rand Corporation, Santa Monica, California, 408 pp.

10. Hourwitz, B., 1948: Insolation in relation to cloud type. Journal of Meteorology, vol. 5, no. 1, pp. 110-113.

11. Haurwitz, B., and J. M. Austin, 1944: Climatology. New York, McGraw-Hill, 410 pp.

12. Houghton, H. G., 1954: On the annual heat balance of the northern hemisphere. Journal of Meteorology, vol. 11, no. 1, pp. 1-9.

13. Joseph, J. H., 1966: Calculation of radiative heating in numerical general circulation models. Tech. Rpt. No. 1, Department of Meteorology, University of California, Los Angeles, pp. 60.

14. Kaitala, J., 1972: Heating and moisture source terms. Manuscript documenting heating terms in the Fleet Numerical Weather Central operational primitive-equation model, pp. 18.

15. Katayama, A., 1966: On the radiation budget of the tropopshere over the northern hemisphere (I). Journal of the Meteorological Society of Japan, vol. 44, no. 6, pp. 381-401.

16. _____, 1967: On the radiation budget of the troposphere over the northern hemisphere (II). Journal of of the Meteorological Society of Japan, vol. 45, no. 2, pp. 1-25.

17. Kesel, P. G. and F. J. Winninghoff, 1972: The Fleet Numerical Weather Central operational primitive-equation model, Monthly Weather Review, vol. 100, no. 5, pp. 360-373.

18. Korb, G., J. Michalowsky and F. Möller, 1956: Investigation on the heat balance of the troposphere. Tech. Rpt. No. 1, Contract AF61(514)-863. 94 pp. (OTS No. PB127016, Obtainable from Library of Congress).

19. Langlois, W. E. and H. C. W. Kwok, 1969: Description of the Mintz-Arakawa numerical general circulation model. Numerical Simulation of Weather and Climate Tech. Rpt. No. 3, Department of Meteorology, University of California.

20. List, R. J., 1958: Smithsonian Meteorological Tables, Smithsonian Institute, Washington, pp. 527.

21. London, J., 1957: A study of the atmospheric heat balance. College of Engineering, New York University. Final report on AFCRL contract 19(122)-165, also issued as AFCRC-TR-57-287.

22. Manabe, S. and F. Möller, 1961: On the radiative equilibrium and heat balance of the atmosphere. Monthly Weather Review, vol. 89, no. 12, pp. 503-522.

23. Manabe, S. and R. F. Strickler, 1964: Thermal equilibrium of the atmosphere with convective adjustment. Journal of the Atmospheric Sciences, vol. 12, no. 4, pp. 361-385.

24. Marlatt, W. E., 1965: The investigation of the temperature and spectral emissivity characteristics of cloud tops and of the earth's surface. Department of Atmospheric Science, Colorado State University, Progress Rpt. under NASA Contract NASr-147.

25. Martin, F. L., 1972: Description of a radiation package for the Naval Postgraduate School general circulation model. Department of Meteorology, Naval Postgraduate School, Monterey, California.

26. Möller, F. and E. Rashke, 1964: Evaluation of TIROS III radiation data. National Aeronautics and Space Administration Contractor Report, NASA CR-112, Washington, D. C., 114 pp.

27. Oliger, J. E., R. E. Wellck, A. Kasahara and W. M. Washington, 1970: Description of the NCAR global circulation model. Tech. note STR-56, National Center for Atmospheric Research, Boulder, Colorado, 94 pp.

28. Posey, J. W. and P. F. Clapp, 1964: Global distribution of normal surface albedo. Geophisica International, Mexico City, pp. 33-48.

29. Sasamori, T., 1968: The radiative cooling calculation for application to general circulation experiments. Journal of Applied Meteorology, vol. 7, no. 5, pp. 721-729.

30. Sellers, W. D., 1965: Physical Climatology. University of Chicago Press, pp. 272.

31. Seinde, R. N., 1954: The distribution of cloudiness by type and height in the northern hemisphere for spring and fall. M. S. thesis, College of Engineering, New York University.

32. Shaw, N., 1936: Manual of Meteorology. Vol. 2 (2nd Ed.), Cambridge University Press.

33. Smagorinsky, J., 1960: On the dynamical prediction of large-scale condensation by numerical methods. Geophysical Monograph, No. 5, American Geophysical Union, Washington, D. C., pp. 71-78.

34. Smith, W. L., 1966: Note on the relationship between total precipitable water and surface dew point. Journal of Applied Meteorology, vol. 5, no. 6, pp. 726-727.

35. Telegadas, K., and J. London, 1954: A physical model for the northern hemisphere troposphere for winter summer. Scientific Rpt. No. 1, Contract AF 19(122)-165, Research Division, College of Engineering, New York University.

36. U. S. Weather Bureau, 1938: Atlas of Climatic Charts of the Oceans. Washington, D. C., Government Printing Office, U. S. Weather Bureau No. 1247, 130 pp.

37. Vowinckel, E. and B. Taylor, 1964: Evaporation and sensible heat flux over Arctic Ocean. Department of Meteorology, McGill University, Montreal. Scientific Rpt. No. 10 under AFCRL contract 19(604)-7415.

38. Yamamoto, G., 1952: On a radiation chart. Sci. Rpts. of the Tohoku Univ., Series No. 4, pp. 9-23.

INITIAL DISTRIBUTION LIST

		No. Copies
1.	Defense Documentation Center Cameron Station Alexandria, Virginia 22314	2
2.	Library, Code 0212 Naval Postgraduate School Monterey, California 93940	2
3.	Professor F. L. Martin, Code 51Mr Department of Meteorology Naval Postgraduate School Monterey, California 93940	6
4.	Lieutenant Robert J. Plante, USN SMC Box 1750 Naval Postgraduate School Monterey, California 93940	2
5.	Department of Meteorology, Code 51 Naval Postgraduate School Monterey, California 93940	1
6.	Assistant Professor R. L. Haney, Code 51Hy Department of Meteorology Naval Postgraduate School Monterey, California 93940	1
7.	Naval Weather Service Command Naval Weather Service Headquarters Washington Naval Yard Washington, D. C. 20390	1

Security Classification

DOCUMENT CONTROL DATA - R & D

(Security classification of title, body of abstract and indexing annotation must be entered when the overall report is classified)

ORIGINATING ACTIVITY (Corporate author)

Naval Postgraduate School
Monterey, California 93940

2a. REPORT SECURITY CLASSIFICATION

Unclassified

2b. GROUP

REPORT TITLE

Tests of a Radiative Transfer Model for Numerical Prediction of the Atmospheric General Circulation

DESCRIPTIVE NOTES (Type of report and, inclusive dates)

Master's Thesis; March 1973

AUTHOR(S) (First name, middle initial, last name)

Robert John Plante

REPORT DATE	7a. TOTAL NO. OF PAGES	7b. NO. OF REFS
March 1973	115	38

CONTRACT OR GRANT NO.	9a. ORIGINATOR'S REPORT NUMBER(S)
b. PROJECT NO.	
c.	9b. OTHER REPORT NO(S) (Any other numbers that may be assigned this report)
d.	

DISTRIBUTION STATEMENT

Approved for public release; distribution unlimited.

SUPPLEMENTARY NOTES	12. SPONSORING MILITARY ACTIVITY
	Naval Postgraduate School Monterey, California 93940

ABSTRACT

An evaluation is performed of a radiation model for the Naval Postgraduate School primitive-equation numerical weather prediction system. The model employs empirical expressions for atmospheric absorptivity, scattering-reflectivity, cloud-reflectivity and earth-surface reflectivity to compute solar insolation absorbed at earth and in the key atmospheric layers. The terrestrial cooling effect at earth and in these same key atmospheric layers is formulated using recent empirically-derived emissivities for the effects of both water vapor and CO_2.

Mean seasonal atmospheric soundings for the Northern Hemisphere are utilized for testing the model. In addition, application of atmospheric boundary-layer modeling permits determination of the surface-layer turbulent transports (in the vertical) of sensible and latent heat at the earth's surface. To evaluate the validity of the radiation model, heat budgets are compiled for the earth-atmosphere system, the atmospheric column and the earth's surface.

DD FORM 1 NOV 65 1473 (PAGE 1)

S/N 0101-807-6811

Security Classification

A-31408

KEY WORDS	LINK A		LINK B		LINK C	
	ROLE	WT	ROLE	WT	ROLE	WT
Oceanic heat transport requirements, Q_{VO}						
Atmospheric heat transport requirements, Q_{VA}						
Humidity profile parameter, λ						
Pressure-scaled absorber masses						
Insolation						
Manabe-Möller absorption						
Flux-emissivity of water vapor and CO_2						
Black-body flux						
Surface boundary conditions						
Primitive equation prediction model						
σ-level surfaces						

Thesis
P612 Plante
c.1
145478
Tests of a radiative transfer model for numerical prediction of the atmospheric general circulation.